Remote Sensing of Environment 279 (2022) 113141

Contents lists available at ScienceDirect

Remote Sensing of Environment

journal homepage: www.elsevier.com/locate/rse

Evaluating the role of solar-induced fluorescence (SIF) and plant physiological traits for leaf nitrogen assessment in almond using airborne hyperspectral imagery

Y. Wang [a,*], L. Suarez [a,b], T. Poblete [a,b], V. Gonzalez-Dugo [c], D. Ryu [a], P.J. Zarco-Tejada [a,b,c]

[a] Department of Infrastructure Engineering, Faculty of Engineering and Information Technology (FEIT), University of Melbourne, Melbourne, VIC 3010, Australia
[b] School of Agriculture and Food, Faculty of Veterinary and Agricultural Sciences (FVAS), University of Melbourne, Melbourne, VIC 3010, Australia
[c] Instituto de Agricultura Sostenible (IAS), Consejo Superior de Investigaciones Cientificas (CSIC), Avenida Menendez Pidal s/n, 14004 Cordoba, Spain

ARTICLE INFO

Edited by Jing M. Chen

Keywords:
Chlorophyll fluorescence
SIF
Nitrogen
Chlorophyll
FluSAIL RTM
Hyperspectral
Gaussian process regression
Random Forest
Almond
Tree orchard

ABSTRACT

Accurate, spatially extensive, and frequent assessments of plant nitrogen (N) enabled by remote sensing allow growers to optimize fertilizer applications and reduce environmental impacts. Standard remote sensing methods for N assessment typically involve the use of chlorophyll-sensitive vegetation indices calculated from multispectral or hyperspectral reflectance data. However, the chlorophyll $a + b$ derived from spectral indices is indirectly related to leaf N and saturates at high leaf N levels, dramatically reducing the sensitivity with leaf N under these conditions. Furthermore, these relationships are heavily influenced by canopy structure, variability in leaf area density, proportion of sunlit-shaded tree-crown components, soil background, and understory. Recent studies in uniform crops have demonstrated that estimation of plant N can be improved by considering leaf biochemical constituents derived from radiative transfer model (RTM) and solar-induced fluorescence (SIF). However, it is unclear whether these methods are transferable to tree crops due to their intrinsic physiological differences, structural complexity, and within-tree crown heterogeneity. We investigated how various hyperspectrally derived proxies for leaf N, including RTM-based traits and SIF, could be combined to assess N status on a 1200-ha almond orchard across two growing seasons. RTM-based chlorophyll $a + b$ content (C_{ab}) and SIF were found to be the most important and consistent predictors for leaf N compared to other leaf biochemical and biophysical traits. C_{ab} alone was a modest predictor of leaf N variability ($r^2 = 0.49$, RMSE = 0.16%, p-value <0.001), but when the non-collinear SIF and C_{ab} traits were coupled together, predictions improved dramatically ($r^2 = 0.95$, RMSE = 0.05%, p-value <0.001). Leaf area index (LAI) was poorly associated with leaf N, suggesting that leaf physiological traits may be more important than structural traits in quantifying leaf N in well-managed orchards characterized by high N levels. Consistent results across the 2 years suggests the importance of airborne SIF coupled with C_{ab} for precision agriculture and leaf N status assessment in almond orchards.

1. Introduction

Nitrogen (N) is an essential nutrient for plant growth, productivity, and quality and is often the major limiting factor for photosynthesis (Evans, 1989). However, more N fertilizer than needed is often applied to maximize yield and quality (Conant et al., 2013). In addition to the economic costs of N over-fertilization, excess N has detrimental effects on the environment, leading to pollution of the atmosphere and water systems (Shcherbak et al., 2014; Stevenson and Cole, 1999; Zebarth et al., 2009). Monitoring crop N status is essential for optimizing N applications and maintaining productivity while minimizing environmental impacts for sustainable agriculture (Manna et al., 2005; Matson et al., 1998; Panhwar et al., 2019; Snyder et al., 2009).

The concentration of leaf nitrogen can be determined through various approaches. The chemical analysis of leaf tissue via destructive sampling, such as the traditional Kjeldahl-digestion method (Kjeldahl, 1883) or the simpler and faster Dumas combustion method to avoid using toxic chemicals (Dumas, 1831), has been the standard method for the assessment of leaf N. Although this approach is very accurate, it is not cost- or time-effective for the continuous monitoring of N status over large areas. In recent decades, imaging spectroscopy has been used as an alternative to lab-based assays from the leaf, enabling rapid N

* Corresponding author.
E-mail address: wang.y@unimelb.edu.au (Y. Wang).

https://doi.org/10.1016/j.rse.2022.113141
Received 13 December 2021; Received in revised form 11 April 2022; Accepted 18 June 2022

monitoring at a range of spatio-temporal scales (Chapman and Barreto, 1997; Dong et al., 2020; Nageswara Rao et al., 2001; Romina et al., 2019; Schepers et al., 1992) to canopy level (Clevers and Gitelson, 2013; Clevers and Kooistra, 2011; Gnyp et al., 2014; Haboudane et al., 2002; Inoue et al., 2012; Nigon et al., 2020; Pinter Jr et al., 2003).

Most remote sensing (RS) studies of leaf N depend on an assumed strong correlation between leaf chlorophyll $a + b$ (C_{ab}) and N (Evans, 1989). Thus, C_{ab} has been proposed as a common RS-based indicator for N assessment (Clevers and Gitelson, 2013; Schlemmer et al., 2013; Wood et al., 1992; Yoder and Pettigrew-Crosby, 1995). The conventional approach in these studies has been to determine an empirical relationship between destructively sampled tissue N and non-destructive proxy measurements, including hand-held spectral readings at visible, red-edge, and near-infrared spectral bands (Bullock and Anderson, 1998; Cerovic et al., 2015; Cerovic et al., 2012; Chang and Robison, 2003; Jongschaap and Booij, 2004; Padilla et al., 2018; Wood et al., 1992) or chlorophyll-sensitive vegetation indices derived from multispectral or hyperspectral reflectance at leaf and canopy levels (Clevers and Gitelson, 2013; Cummings et al., 2021; Filella et al., 1995; Fitzgerald et al., 2010; Gnyp et al., 2014; Inoue et al., 2012; Nigon et al., 2020). Although leaf chlorophyll meters are valuable tools for quick on-farm determination of leaf N status, the relationship between chlorophyll meter readings and N content differs across plant genotypes and environmental contexts (Xiong et al., 2015). Furthermore, these chlorophyll indicators from chlorophyll meters or vegetation indices are not the actual chlorophyll content, but rather the proxy for leaf greenness. Although they are generally related to leaf N, these proxies saturate at high N levels, resulting in reduced sensitivity to increased N values (Li et al., 2020; Padilla et al., 2018; Romina et al., 2019; Schlemmer et al., 2013). In addition to these leaf greenness indicators, vegetation indices widely used in RS such as the Normalized Difference Vegetation Index (NDVI) (Rouse et al., 1974), are also indirectly related to N (Yoder and Pettigrew-Crosby, 1995). They have been demonstrated to lack sensitivity and to saturate at high plant densities and under overfertilization levels (Flowers et al., 2003; Matsushita et al., 2007; Nguy-Robertson et al., 2012). To prevent these effects, proxies directly linked to leaf N through pathways other than via the quantification of chlorophyll content are required.

Moreover, spectral indices that incorporate red-edge spectra are thought to be improved ways to derive N status due to the higher sensitivity of this spectral region to moderate and high chlorophyll content levels (Gitelson et al., 2003; Gitelson et al., 1996). Fitzgerald et al. (2006) found that the Normalized Difference Red-Edge (NDRE) index, which is calculated by replacing the red band of NDVI with the red-edge band, was a reliable indicator of chlorophyll *a*nd N status. Another index termed the Canopy Chlorophyll Content Index (CCCI) is based on a two-dimensional planar extension of NDVI and NDRE and has been proposed as a method for improved estimation of N in annual crops (e.g., wheat (*Triticum aestivum*)) (Fitzgerald et al., 2010; Li et al., 2014; Perry et al., 2012). Another approach combining the information in the red-edge with a structural index is the use of the Transformed Chlorophyll Absorption in Reflectance Index (TCARI) with the Optimized Soil-Adjusted Vegetation Index (TCARI/OSAVI) (Haboudane et al., 2002). These indices tend to be sensitive to chlorophyll $a + b$ induced by N variability while also accounting for background effects (Gabriel et al., 2017; Wu et al., 2008). Nevertheless, empirical relationships are required to estimate N from these vegetation indices.

As leaf N content is associated with many other physiological traits besides C_{ab} content, the use of radiative transfer model (RTM)-based retrievals of plant physiological traits is a promising alternative to spectral indices for assessing leaf N. Due to the fact that leaf N is not an input in the RTM, nutrient variability was described through a wide range of model-simulated plant traits, including leaf constituents (e.g., C_{ab}, dry matter (C_{dm}), water content (C_w)), and canopy structural parameters (Baret et al., 2007; Camino et al., 2018a; Thorp et al., 2012; Wang et al., 2021; Wang et al., 2018). Traits derived from RTMs are considered more accurate and transferrable than index-based empirical algorithms (Kimes et al., 2000), although this has only been tested for uniform crops. For orchards, this method is more complex due to the tree crown heterogeneity and clumping effects with mixed crown-shadow-soil backgrounds. Radiative transfer model inversion also allows inverting for other non-photosynthetic plant pigments, such as carotenoids (C_{car}) and xanthophylls (C_x), which are involved in photosynthetic light-harvesting (Jacquemoud et al., 2009; Niyogi et al., 1997; Vilfan et al., 2016; Vilfan et al., 2018). Plants prevent photodamage by deoxidizing the xanthophyll violaxanthin (V) into antheraxanthin (A) and zeaxanthin (Z) in response to excess excitation energy (Demmig et al., 1987; Gilmore, 1997). Therefore, xanthophyll composition is linked to photosynthetic efficiency and may thus relate to leaf N status, particularly under abiotic stress conditions (Cheng, 2003; Ramalho et al., 2000; Tóth et al., 2002; Verhoeven et al., 1999). Thus, based on their links with photosynthesis under stress conditions, the complete set of photosynthetic and non-photosynthetic pigments, along with structural traits, can lead to a more informed assessment of N.

In the last few decades, solar-induced fluorescence (SIF) has been proposed as a trait for monitoring plant physiology, vegetation functioning, and plant biotic and abiotic stress detection due to the dynamic changes in photochemical and non-photochemical quenching in the photosynthetic process (see review paper by Mohammed et al. (2019) and studies from Maxwell and Johnson (2000); Mohammed et al. (1995); Murchie and Lawson (2013); Porcar-Castell et al. (2014); Sayed (2003); Zarco-Tejada et al. (2018)). It is well known that abiotic-induced stress conditions such as light intensity, water status, and temperature extremes modulate the photosynthetic performance (Ashraf and Harris, 2013; Biswal et al., 2011; Saibo et al., 2009). Most importantly, SIF is considered a direct proxy for electron transport rate and thus a direct measure of photosynthesis (Genty et al., 1989; Krause and Weis, 1991; Middleton et al., 2016; Walker et al., 2014). N modulates the fluorescence-photosynthesis link, thus several studies propose SIF as a potential proxy for the assessment of leaf N status at both the leaf (Huang et al., 2004; Lu and Zhang, 2000) and the canopy levels (Cendrero-Mateo et al., 2016; Corp et al., 2003; Middleton et al., 2016; Mohammed et al., 2019; Wang et al., 2021). For example, Camino et al. (2018a) showed that SIF improved predictions of N content in wheat. However, in tree orchards, SIF is affected by canopy structure and the mixing of within-crown sunlit and shaded components. This adds complexity to the accurate SIF quantification in tree orchards (Camino et al., 2018b). The combined use of RTM-based leaf biochemistry estimates with SIF for N assessment is poorly studied in structurally complex tree orchards. Such a methodology may have important uses in precision agriculture when using commercial hyperspectral sensors with 5- to 6-nm spectral resolution, which have been shown to be sensitive to SIF emission and thus are useful for quantifying abiotic sources of stress (Belwalkar et al., 2022; Belwalkar et al., 2021; Raya-Sereno et al., 2021; Zarco-Tejada et al., 2016; Zarco-Tejada et al., 2012; Zarco-Tejada et al., 2013).

In this study, we explored the contribution of various hyperspectrally derived proxies for leaf N status assessment in almond orchards across two consecutive growing seasons, including airborne-quantified plant physiological traits estimated by RTM inversion and canopy SIF. We evaluated the accuracy and robustness of the retrieved plant physiological traits and the collinearity among plant pigments, SIF, and structural traits when assessing leaf N variability across the field. Rather than a data driven approach, our study advances the mechanistic understanding of the responses of RS-derived plant traits to leaf N content changes.

2. Material and methods

2.1. Study area and field data collection

This study was conducted in a commercial almond orchard in

northwest Victoria, Australia, at the pre-harvest stage of the growing season in 2019/2020 and 2020/2021 when the leaves are mature and have reached their maximum N uptake capacity. The region has a Mediterranean climate with hot, dry summers and mild, wet winters. Average annual precipitation is 300 mm. The summer of 2020/2021 was milder than that of 2019/2020, with an average maximum air temperature of 29.5 °C in December 2020, compared to 34.3 °C in December 2019. The almond orchard (Fig. 1) covers approximately 1240 ha with trees planted between 2006 (Northern blocks facing N-S) and 2007 (Southern blocks mixed in N-S and *E*-W orientations) on sandy loam soils. Generally, trees planted in the eastern blocks tend to have larger tree crowns than those in the west. Three almond varieties were planted in alternating blocks of six rows to facilitate cross-pollination (Asai et al., 1996; Hill et al., 1985). Varieties included Nonpareil (50%), Carmel (33%), and Price (17%). A drip fertigation system was used to supply the same amount of water and nutrients to the tree root zones for each variety at the same time and was established at 1-h intervals between varieties across the entire orchard. Fertigation was supplied as needed based on weather and plant responses over the growing season. In summer of 2020/2021, irrigation volume was 10% higher (12,795 m^3/ha) than in 2019/2020 (11,465 m^3/ha), but total N fertilizer applications (330 kg/ha in 2020/2021 and 326 kg/ha in 2019/2020) were similar. In summer of 2020/2021, Nonpareil was treated with 10% less fertigation than Carmel and Price varieties across the orchard based on the difference observed along the 2019/2020 season.

Fifteen homogeneous plots consisting of six rows of seven to eight trees were monitored throughout the experiment in 2019/2020 and 2020/2021 (Fig. 2). In each plot, four adjacent trees from Nonpareil and Carmel varieties (two each; yellow dashed rectangle in Fig. 2a) were sampled in situ prior to harvest in both years. Leaf C_{ab}, anthocyanins (Anth), flavonoid (Flav) content, and the nitrogen balance index (NBI) were measured from 20 representative sunlit mature leaves per tree using a Dualex 4 Scientific sensor (FORC*E*-A, Orsay, France). Leaf steady-state chlorophyll fluorescence (Ft) and leaf reflectance spectra within the visible (VIS) and near-infrared (NIR) regions were measured with FluorPen FP 110 and PolyPen RP 410 instruments (PSI, Brno, Czech Republic) on the same leaves with the Dualex sensor. A series of vegetation pigment indices (see Table 1 for the complete list of indices used in this study) were calculated based on the leaf reflectance spectra measured from the PolyPen handheld instrument. An additional set of 20 leaves per plot were collected for biochemical laboratory analyses using Dumas Combustion (Buckee, 1994; Dumas, 1831; Etheridge et al., 1998) with a LECO TruMac CNS Macro Analyzer (LECO Corporation, MI, USA) and an inductively coupled plasma optical emission spectrometer (ICP-OES Optima 8300, Perkin Elmer, USA). Thirteen macro and micronutrients (e.g., nitrogen, carbon, phosphorus, and potassium) were measured. The ranges of variation of field data collected over 2 years were compared against Ft-measured quartiles. The correlations between leaf measurement and laboratory N concentration were calculated for both years.

Fig. 1. Colour-infrared (CIR) overview of the hyperspectral mosaic acquired with the VNIR hyperspectral sensor over the 1200-ha study site collected on January 31, 2021. Spectral bands at 860 (R), 650 (G), and 550 (B) nm are shown with a spatial resolution of 40 cm per pixel.

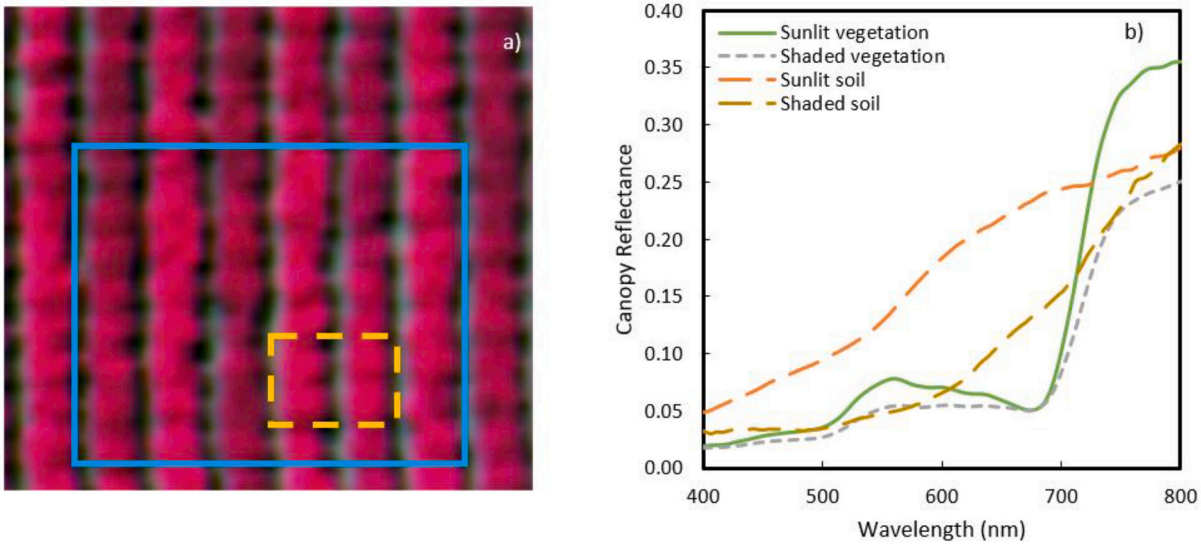

Fig. 2. (a) Study plot consisting of six rows by eight trees within the blue solid line. Leaves from four trees within the yellow dashed rectangle were measured in the field. (b) The reflectance spectra of different scene components extracted from the airborne hyperspectral imager, including sunlit (green solid line) and shaded (grey dashed line) tree crown, and sunlit (orange dashed line) and shaded soil (brown dashed line) pixels. (For interpretation of the references to colour in this figure legend, the reader is referred to the web version of this article.)

Table 1
Spectral vegetation index equations used in this study.

Index	Equation	Reference
Structural indices		
NDVI	$(R_{800} - R_{670})/(R_{800} + R_{670})$	Rouse et al. (1974)
EVI	$2.5 \bullet (R_{800} - R_{670})/(R_{800} + 6 \bullet R_{670} - 7.5 \bullet R_{500} + 1)$	Liu and Huete (1995)
MCARI2	$1.5 \bullet (2.5 \bullet (R_{800} - R_{670}) - 1.3 \bullet (R_{800} - R_{550})) \Big/ \sqrt{(2 \bullet R_{800} + 1)^2 - (6 \bullet R_{800} - 5 \bullet R_{670}) - 0.5}$	Haboudane et al. (2004)
RDVI	$(R_{800} - R_{670})/\sqrt{R_{800} + R_{670}}$	Roujean and Breon (1995)
OSAVI	$(1 + 0.16) \bullet (R_{800} - R_{670})/(R_{800} + R_{670} + 0.16)$	Rondeaux et al. (1996)
Chlorophyll a + b indices		
MCARI	$((R_{700} - R_{670}) - 0.2 \bullet (R_{700} - R_{550})) \bullet (R_{700}/R_{670})$	Daughtry et al. (2000)
TCARI/OSAVI	$3 \bullet ((R_{700} - R_{670}) - 0.2 \bullet (R_{700} - R_{550}) \bullet (R_{700}/R_{670})) / (1 + 0.16) \bullet (R_{800} - R_{670})/(R_{800} + R_{670} + 0.16)$	Haboudane et al. (2002)
NPQI	$(R_{415} - R_{435})/(R_{415} + R_{435})$	Barnes et al. (1992)
PSSRa	R_{800}/R_{675}	Blackburn (1998)
PSSRb	R_{800}/R_{650}	Blackburn (1998)
PSSRc	R_{800}/R_{500}	Blackburn (1998)
SIPI	$(R_{800} - R_{445})/(R_{800} - R_{680})$	Penuelas et al. (1995)
CTRI1	R_{695}/R_{420}	Carter (1994)
Indices based on the green region		
PRI	$(R_{570} - R_{531})/(R_{570} + R_{531})$	Gamon et al. (1992)
PRI_{515}	$(R_{515} - R_{531})/(R_{515} + R_{531})$	Hernández-Clemente et al. (2011)
PRI•CI	$((R_{570} - R_{531})/(R_{570} + R_{531})) \bullet ((R_{760}/R_{700}) - 1)$	Garrity et al. (2011)
Fluorescence quantification		
SIF	$E_{out} \cdot L_{in} - E_{in} \cdot L_{out} / E_{out} - E_{in}$ Where E and L represent the incoming irradiance and canopy radiance, 'in' band refers to 762 nm, and 'out' band refers to the average value in 750 and 778 nm	Plascyk and Gabriel (1975)
Canopy temperature		
CWSI	$(T_c - T_a) - (T_c - T_a)_{LL} / (T_c - T_a)_{UL} - (T_c - T_a)_{LL}$ Where LL and UL represent the upper limit and lower limit of canopy (T_c) and air (T_a) temperatures	Jackson et al. (1981)

2.2. Airborne hyperspectral and thermal imagery

Airborne campaigns were conducted concurrently with the field measurements on February 17, 2020, and January 31, 2021. Both campaigns occurred at solar noon under clear skies. Field sampling and auxiliary data collection required for the calibration and atmospheric correction of the images were conducted simultaneously with airborne campaigns. A hyperspectral line-scanning sensor (Micro-Hyperspec VNIR E-Series model, Headwall Photonics, Fitchburg, MA, USA) and a thermal infrared camera (A655sc model, FLIR Systems, Wilsonville, OR, USA) were flown in tandem on a manned aircraft operated by the HyperSens Remote Sensing Laboratory, the Airborne Remote Sensing Facility of The University of Melbourne. The hyperspectral imager covers 371 spectral bands in the visible and near-infrared regions (400–1000 nm) with a full-width at half-maximum (FWHM) of 5.8 nm and a spectral sampling interval of 1.626 nm. Hyperspectral and thermal images with an angular field of view (FOV) of 66° and 45° (8- and 13.1-mm focal length), respectively, were collected by the aircraft at 550 m above ground level (AGL), yielding spatial resolutions of 40 and 60 cm, respectively, enabling the differentiation of sunlit and shaded components of tree crowns and soil areas. SMARTS (Gueymard, 1995, 2001; Gueymard et al., 2002) irradiance simulations were used to correct for atmospheric effects of the hyperspectral imagery based on aerosol optical measurements at 500 nm taken with a Microtops II sunphotometer (Solar Light, PA, USA) connected to a GPS – 12 navigator (Garmin, Olathe, KS, USA) at the time of each flight. Air temperatures and relative humidity were calculated based on the average of three nearby weather stations (Robinvale, Lake Powell and Wemen) less than 15 km from the study site. Hyperspectral line-scanned image orthorectification was performed using PARGE software (ReSe Applications Schläpfe, Wil, Switzerland) with readings from the onboard inertial measuring unit (IMU) (VectorNav VN-300 dual-antenna GNSS/INS, Dallas, TX, USA). Empirical line calibration was conducted by measuring the reflectance spectra and temperature of bare soil and green and dry vegetation. Spectra were measured with an ASD Handheld-2 field spectrometer (FieldSpec Handheld Pro, ASD Inc., CO, USA), and temperature was measured with a thermal gun (LaserSight, Optris, Germany). Hyperspectral and thermal imagery were mosaicked (Figs. 1 and 3) using ENVI (Boulder, Colorado) and Pix4D (Lausanne, Switzerland) photogrammetry software, respectively.

Automatic segmentation of the hyperspectral reflectance imagery was conducted using Fiji (Abràmoff et al., 2004) combining Niblack's (Niblack, 1985) thresholding method on the NIR band, and Phansalkar's thresholding method (Phansalkar et al., 2011) on a structural index (NDVI >0.72). This method enabled the discrimination of sunlit pure tree crowns from the soil background, as well as the separation of within-crown shadows (see reflectance spectra in Fig. 2b). Considering the sensitivity of SIF to the illumination levels, a more selective segmentation (10% restricted) was applied to the hyperspectral radiance data when segmenting the sunlit crown component. The thermal

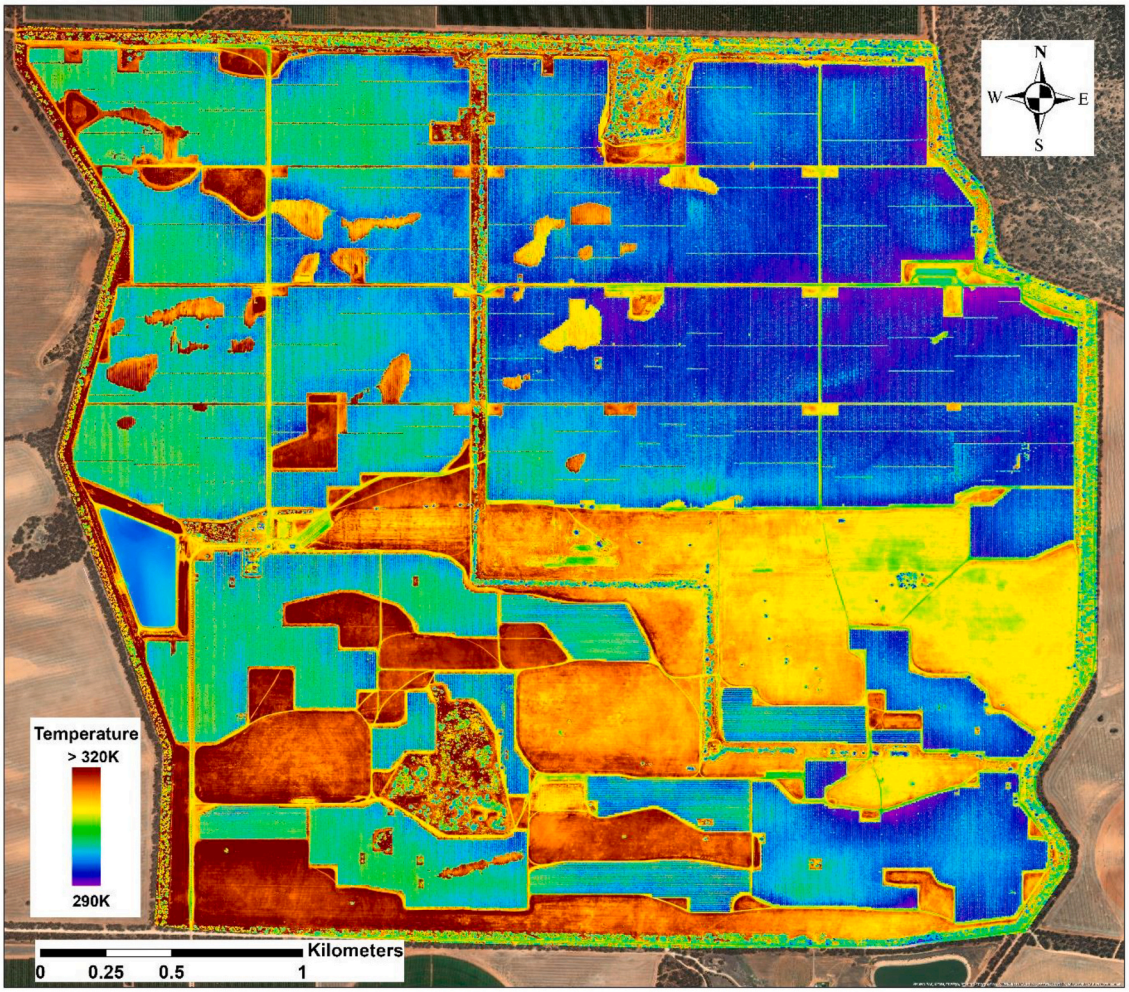

Fig. 3. Thermal mosaic collected over the entire study area captured on January 31, 2021 at a spatial resolution of 60 cm. Cooler colors (purple and blue) indicate plant canopies, and yellow/brown colors indicate soil. (For interpretation of the references to colour in this figure legend, the reader is referred to the web version of this article.)

segmentation of the tree canopy was performed with Niblack's thresholding method (Niblack, 1985) to eliminate the soil and background effects. The resulting pure vegetation pixels obtained in the previous step were clustered into tree-crown features using a watershed segmentation approach based on Euclidean distance (as in Zarco-Tejada et al. (2018)). In Fig. 4, an example of the segmentation conducted on the hyperspectral and the thermal mosaics is presented.

The mean radiance and reflectance spectra, and temperature were extracted from tree crown pixels by hyperspectral and thermal imagery for each study plot. The crop water stress index (CWSI) (Idso et al., 1981) was calculated based on the canopy-air temperature difference and the water vapor pressure deficit (VPD) at the time of image acquisition for assessing the tree-crown water stress levels. A non-water-stressed baseline (NWSB) for almond trees suggested by Bellvert et al. (2018) was used.

SIF was quantified using the Fraunhofer line depth (FLD) principle (Plascyk and Gabriel, 1975) based on three spectral bands (3FLD) (Maier et al., 2004) located inside and outside the O_2-A absorption features. Specifically, we compared canopy radiance values L_{in} at 762 nm and L_{out} at 750 and 778 nm extracted from the hyperspectral imagery to the corresponding incoming irradiance E_{in} (E_{762}) and E_{out} (E_{750}, E_{778}) derived from the field measurements during the flight and resampled to match the spectral specifications of the airborne hyperspectral sensor. To account for the effects of negative values from atmospheric and calibration factors, SIF was scaled using the offset from non-fluorescence targets (e.g., soil) extracted from the imagery. Fig. 5 shows the irradiance and the mean radiance spectra from two study plots (in Fig. 5a and b) at the oxygen-A absorption region around 760 nm. Average tree-crown reflectance (R) spectra extracted from pure vegetation pixels were used to estimate plant traits through RTM inversion and to calculate narrow-band hyperspectral indices (Table 1) for comparison. The set of indices used comprised structural indices (e.g., NDVI), pigment indices (e.g., Modified Chlorophyll Absorption in Reflectance Index (MCARI), TCARI/OSAVI, and Carter Index 1 (CTRI1)), and indices in the visible region (e.g., Photochemical Reflectance Index (PRI)) that track the dynamics of photoprotective mechanisms. Indices calculated

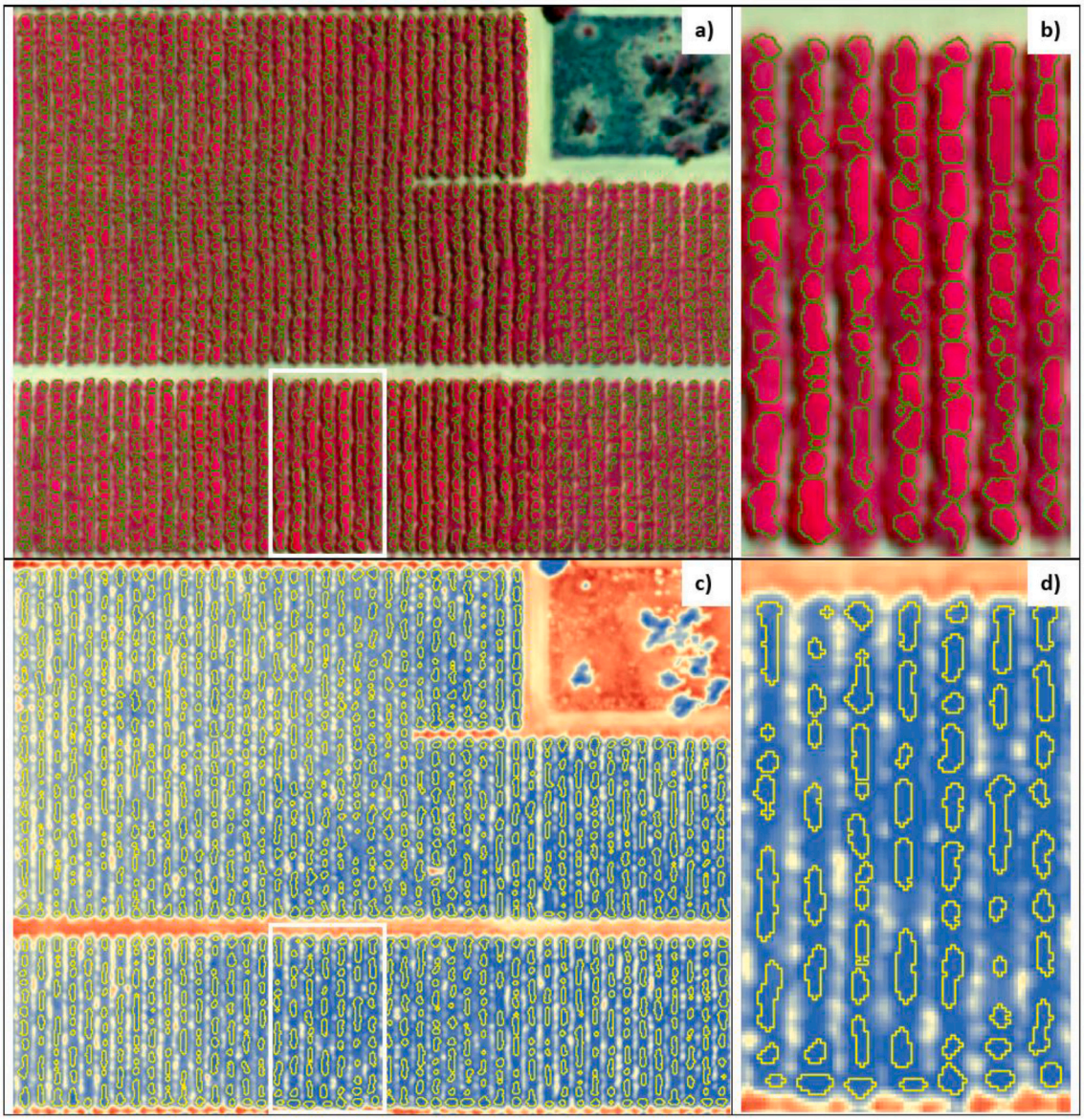

Fig. 4. Overview of the tree-crown segmentation applied to the hyperspectral mosaic (a, upper image in colour-infrared, crown in green outline) and the thermal mosaic (c, bottom image displaying cooler canopy in blue and hot soil in red colour, crown in yellow outline). Right column contains zoomed-in views (b and d) of the scenes within the white rectangle on the left. (For interpretation of the references to colour in this figure legend, the reader is referred to the web version of this article.)

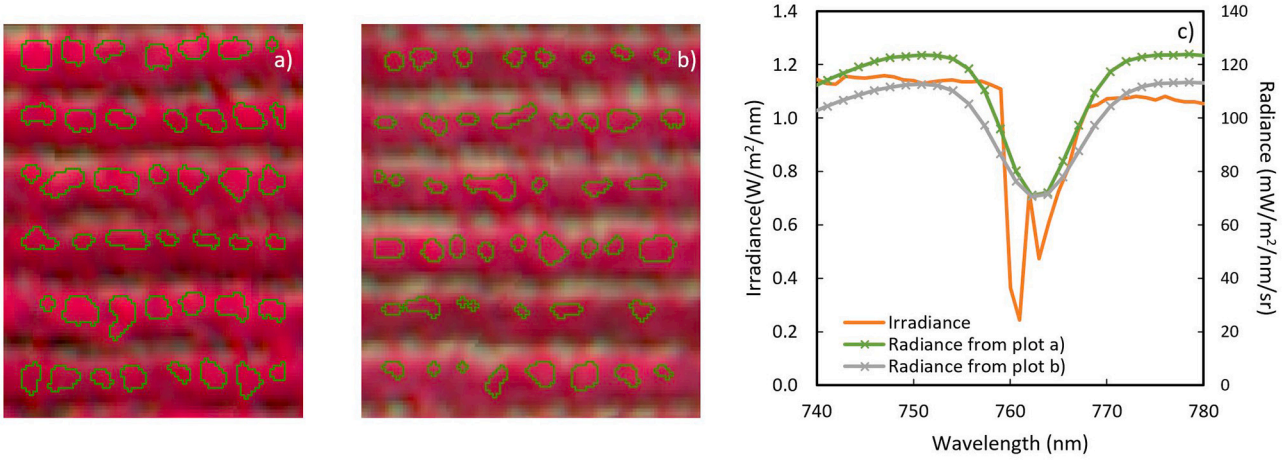

Fig. 5. Segmentation of the sunlit crown area for SIF quantification on two study plots (a) higher nutrient level and (b) lower nutrient level. The irradiance spectrum (orange colour) was used along with the radiance spectra (example shown in (c) for two study plots (green and grey lines) to calculate SIF. Crosses denote the spectral position of the sensor bands (c). (For interpretation of the references to colour in this figure legend, the reader is referred to the web version of this article.)

from airborne imagery were also compared against leaf N, C_{ab}, NBI, and Ft measured in the field.

2.3. Modeling methods for plant trait retrieval and N assessment

The coupled leaf-level Fluspect-Cx model (Vilfan et al., 2018) and 4SAIL (Verhoef, 1984) canopy radiative transfer model, referred to here as FluSAIL, were employed to derive plant biophysical and biochemical parameters by inverting the average canopy reflectance extracted from pure vegetation pixels. The de-epoxidation state of the xanthophyll cycle (C_x) as well as C_{ab}, C_{car}, and Anth pigment content were retrieved by the inversion of the Fluspect-Cx model. A look-up table (LUT) was generated by running 50,000 simulations using randomly generated input parameters drawn from uniform distributions (Table 2). Parameter ranges were adjusted for the viewing geometries due to the slightly different solar zenith angles (SZAs) for each airborne dataset. Biochemical constituents and biophysical parameters were estimated simultaneously for all study plots using a 10-hidden layer artificial neural network (ANN) model (Combal et al., 2003; Hassoun, 1995). The model was trained using 70% of the LUT spectra and tested using the remaining 30% with the mean squared error (MSE) as a performance measure. The model was fit in MATLAB (MATLAB; Statistics and Machine Learning Toolbox and Deep Learning Toolbox; Natick, Massachusetts, USA). Retrieved parameters were used to simulate reflectance spectra with the FluSAIL model using the retrieved parameters and compared with the observed reflectance spectra obtained from the imagery in the 400–900-nm range based upon the root-mean-square deviation (RMSE) assessment. Additionally, the correlations of field leaf-level measurements against estimated plant traits derived from the inversion of the FluSAIL model were compared with those obtained from hyperspectral indices.

To predict leaf N concentration, a pool of representative plant traits and parameters was considered as inputs in the N model, including (1) leaf biochemical and canopy biophysical traits retrieved from pure reflectance spectra with FluSAIL model inversion, (2) airborne-quantified SIF from sunlit-crown radiance spectra, and (3) the water stress indicator CWSI calculated from the thermal imagery. Random Forest (Breiman, 2001) and Gaussian process regression (Williams and Rasmussen, 1996, 2006) algorithms were built with fine-tunning of hyperparameter optimization with 1000 iterations incorporated in the leave-one-out-cross-validation (LOOCV, 15-fold) training and testing steps for each year's dataset. Previously, input collinearity was evaluated using the variance inflation factor (VIF) analysis (O'brien, 2007) following the approach in Zarco-Tejada et al. (2018) conducted using the 'fmsb' package (Gareth et al., 2013) in R. Out-of-bag (OOB) predictor importance was implemented to rank the input relative contribution to the models (as in Zarco-Tejada et al. (2021)). Input parameters with a high degree of collinearity (VIF > 5) (Akinwande et al., 2015) and therefore less informative contribution were filtered out to avoid redundancy. Both Random Forest and Gaussian process regression models were evaluated using the final selection of input parameters. The model performance was evaluated based on the coefficient of determination (r^2) and RMSE. In addition, models with different combination of any two non-collinear parameters were evaluated. In particular, models using leaf biochemical constituents and biophysical parameters with and without SIF were compared to assess the contribution of SIF to N

Table 2
Ranges of input parameters for the LUT of FluSAIL model.

Parameter	Symbol	Unit	Range/ Value
Leaf thickness and constituents			
Chlorophyll $a + b$ content	C_{ab}	µg/ cm^2	20–70
Carotenoid content	C_{car}	µg/ cm^2	3–20
Anthocyanin content	Anth	µg/ cm^2	0–10
Leaf water content	C_w	g/ cm^2	0.001–0.05
Leaf dry matter content	C_{dm}	g/ cm^2	0.001–0.05
Brown pigment content	C_s	µg/ cm^2	0
Leaf mesophyll structural parameter	N-struct	–	1.3–2.5
Leaf dynamic biochemistry			
De-epoxidation state of the xanthophyll cycle (photochemical reflectance parameter)	C_x	–	0–3
Fraction of photons partitioned to PSI	$f_{qe}I$	–	0.002
Fraction of photons partitioned to PSII	$f_{qe}II$	–	0.02
Canopy structural parameters			
Leaf area index	LAI	m^2/ m^2	1–7
Hot spot parameter	q	–	0.03
Leaf inclination distribution function parameter *a*	$LIDF_a$	–	−1–1
Leaf inclination distribution function parameter *b*	$LIDF_b$	–	−1–1

assessments.

A final evaluation was conducted with the LOOCV (30-fold) method using the non-collinear airborne-quantified C_{ab} and SIF for N assessment from both datasets. Model performance was determined using r^2 and RMSE against the validation data from the 2 years. The best Gaussian process regression model was applied at the tree-crown level to obtain the spatial variability of the tree-based N concentration for the entire 1200-ha almond orchard using the airborne-quantified SIF and C_{ab} content from FluSAIL RTM inversion. The continuous map of N concentration for each management unit were generated using the Kernel interpolation with barriers (KIB) algorithm (Worton, 1989) in ESRI ArcGIS Desktop (Redlands, CA, USA) to visualize the variability across the entire orchard.

3. Results

3.1. Field and laboratory data analyses

Leaf nutrient and pigment content varied widely within the study site and across the two growing seasons. Mean leaf N concentration was 2.07% in 2020 and 2.36% in 2021. The Dualex measured C_{ab} and Flav were more variable in 2021 than in 2020. Mean C_{ab} was 32.53 units in 2020 and 30.71 units in 2021. Mean Flav was 2.04 units in 2020 and 1.84 units in 2021. Anth range was higher in 2021 than in 2020, with a mean value of 0.24 units compared to 0.19 in 2020. NBI was 16.46 in 2020 and 17.18 in 2021. Ft was highly variable throughout the orchard and was higher in 2021 than in 2020, ranging from 1648 to 2751 units in 2020 and from 2574 to 3970 units in 2021.

The relationships between leaf steady-state chlorophyll fluorescence quartiles and derived spectral and physiological metrics varied across seasons (Fig. 6). Similar linear relationships were observed across seasons for leaf N concentration (Fig. 6a), Flav (Fig. 6c), NBI (Fig. 6d), and leaf spectral indices (Fig. 6f-i). By contrast, Anth (Fig. 6e) exhibited opposite trends with Ft quartiles between 2020 (negative) and 2021 (positive). Unexpectedly, leaf C_{ab} (Fig. 6b) did not exhibit consistent trends relative to leaf Ft quartiles, with generally positive and negative trends for 2020 and 2021 (n.s.), respectively.

In general, leaf measurements were correlated with each other across years (Fig. 7). Chlorophyll content and leaf N were strongly correlated in 2020 ($r^2 = 0.60$, p-value <0.005, Fig. 7a). However, this correlation was not statistically significant in 2021 ($r^2 = 0.04$, n.s.). Leaf N was more consistently correlated with Dualex-measured NBI (Fig. 7b) for both

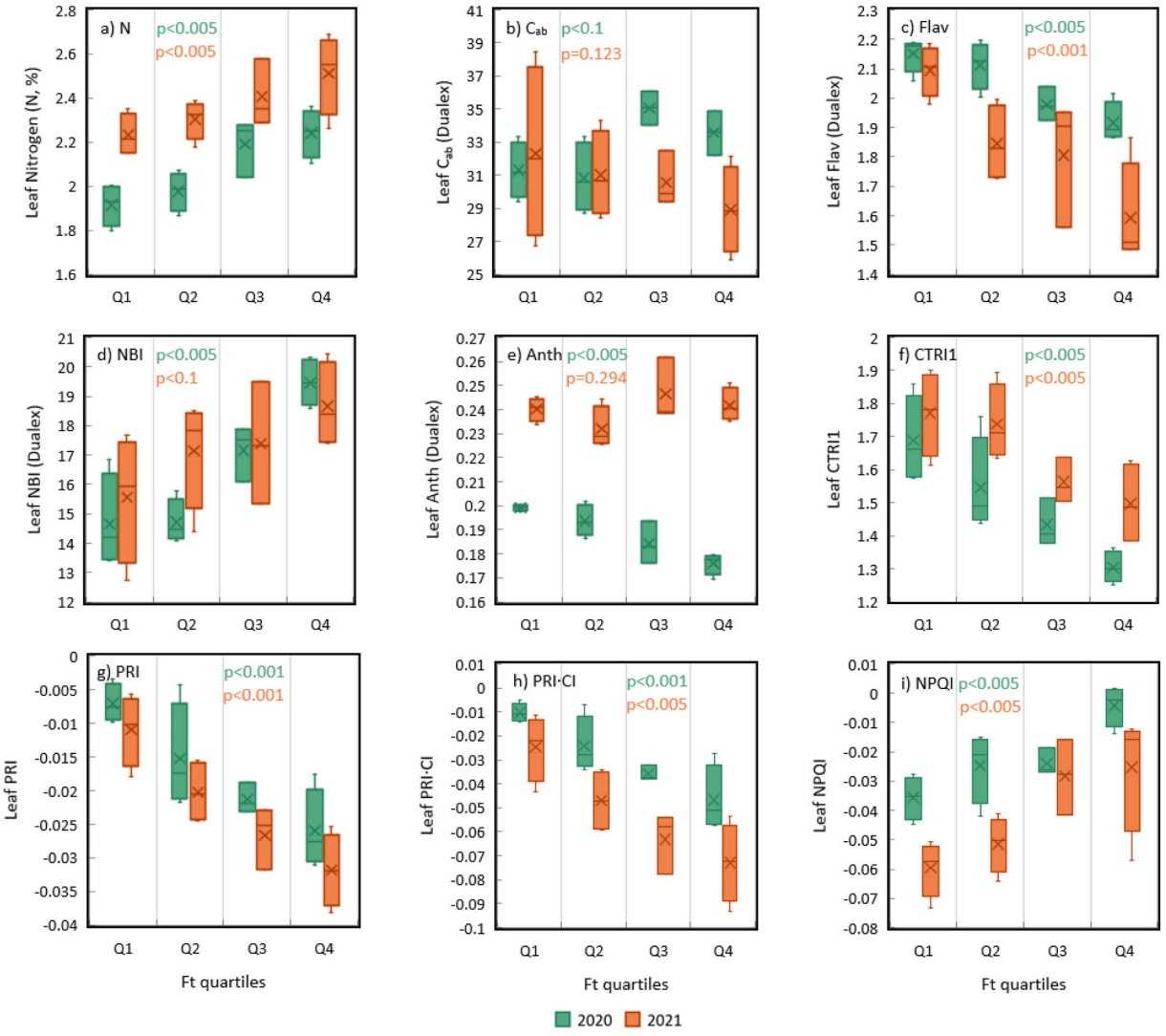

Fig. 6. Ranges of variation based on leaf steady-state chlorophyll fluorescence (Ft) quartiles for leaf phenotypes measured at the pre-harvest stage in 2020 (green) and 2021 (orange): a) nitrogen concentration, b) chlorophyll $a + b$ (C_{ab}), c) flavonoid (Flav), d) Nitrogen Balance Index (NBI), e) anthocyanins (Anth), f) CTRI1, g) PRI, h) PRI•CI, and i) NPQI. The line through the box and marker 'x' refer to the median and mean value, respectively. (For interpretation of the references to colour in this figure legend, the reader is referred to the web version of this article.)

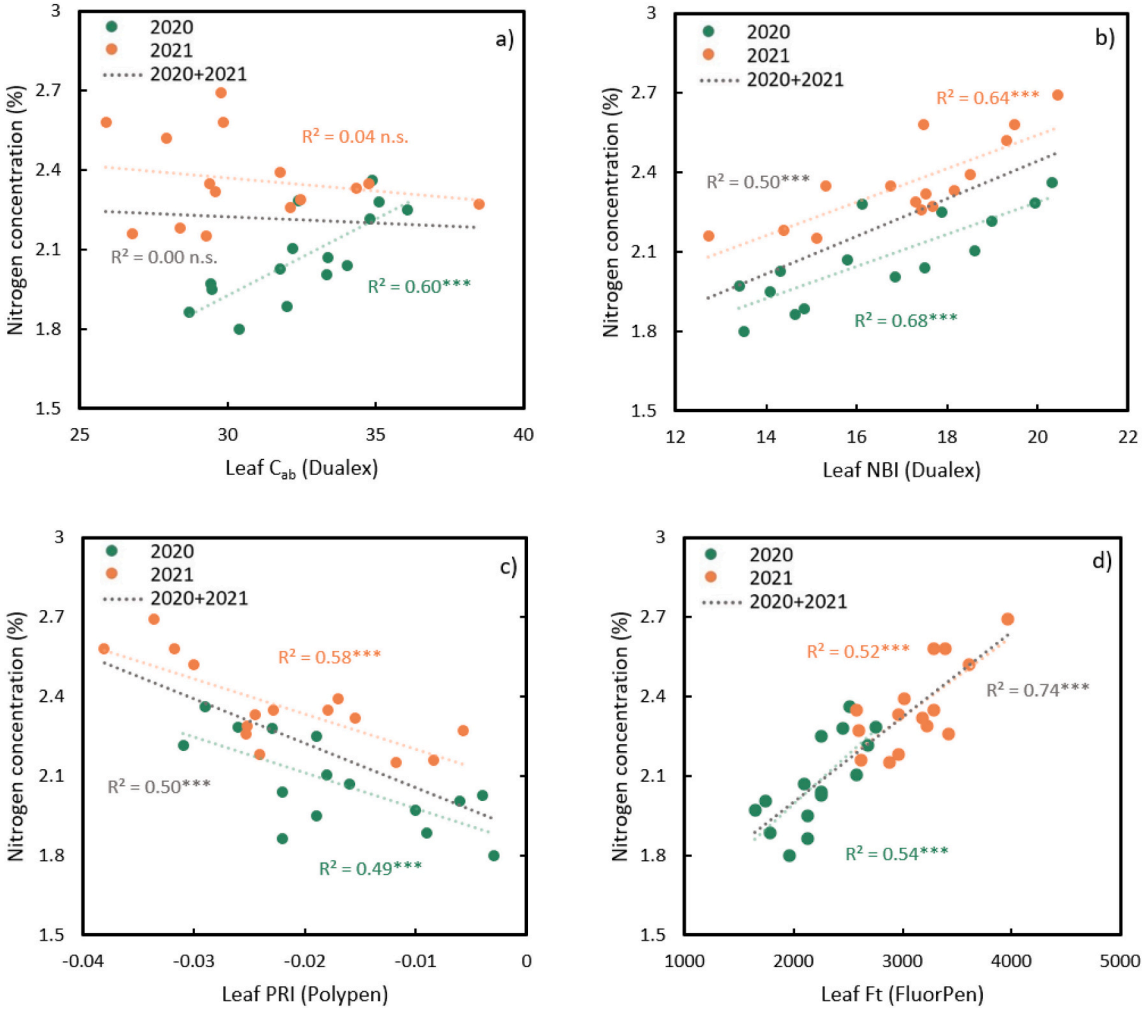

Fig. 7. Relationships between leaf N concentration (%) and a) leaf chlorophyll content, b) Nitrogen Balance Index (NBI), c) photochemical reflectance index (PRI), and d) steady-state chlorophyll fluorescence (Ft). Green and orange represent data in 2020 and 2021, respectively. Grey is used to represent correlation when combining data of 2 years. *p-value <0.05; **p-value <0.01; ***p-value <0.005; n.s. = not significant. (For interpretation of the references to colour in this figure legend, the reader is referred to the web version of this article.)

years ($r^2 = 0.68$ for 2020 and $r^2 = 0.64$ for 2021; p-values <0.005), since the index calculation incorporates both chlorophyll *a*nd flavonoids. Leaf PRI (related to xanthophyll composition changes) was also correlated with leaf N across seasons ($r^2 = 0.49$ in 2020 and $r^2 = 0.58$ in 2021; p-values <0.005, Fig. 7c) as was Ft ($r^2 = 0.54$ in 2020 and $r^2 = 0.52$ in 2021; p-values <0.005, Fig. 7d). Leaf fluorescence (Fig. 7d) was strongly correlated with N when using combined 2-year data ($r^2 = 0.74$, p-value <0.005), outperforming the rest of the leaf traits (e.g., $r^2 = 0.50$ for PRI and NBI; p-values <0.005).

3.2. *Narrow-band indices calculated from airborne hyperspectral imagery*

Relationships between narrow-band reflectance indices, airborne SIF, and field-based leaf measurements are summarized in Table 3. The results present a wide range of correlation and significance levels between leaf physiological measurements and indicators of canopy structure, pigments, airborne-quantified fluorescence, and CWSI temperature-based stress indicator. Airborne-quantified SIF (Fig. 8a) was significantly correlated with Ft in both 2020 ($r^2 = 0.73$, p-value <0.005) and 2021 ($r^2 = 0.30$, p-value <0.05). The relationship was stronger when combining datasets across 2 years ($r^2 = 0.77$, p-value <0.005; shown by the grey dashed line in Fig. 8). SIF was also significantly correlated with leaf N ($r^2 = 0.60$ in 2020 and 0.55 in 2021, p-values <0.005), and the relationships remained strong when combining data from both years ($r^2 = 0.74$, p-value <0 0.005, Fig. 8b). Strong correlations were also evident between SIF and leaf NBI ($r^2 = 0.46$ and 0.67, p-values <0.01) in 2020 and 2021, respectively. Fluorescence, as a proxy of photosynthesis, both at the leaf (Fig. 7d) and canopy levels (Fig. 8b), achieved steady and strong relationships with leaf N ($r^2 = 0.74$, p-value <0.005).

Hyperspectral indices related to vegetation structure (e.g., NDVI) and pigment concentration (e.g., MCARI) were generally correlated with leaf chlorophyll measured by Dualex in 2020, but not in 2021 (Table 3). This pattern was reversed for leaf NBI, where canopy structure (e.g., EVI) and pigment indices (e.g., MCARI) were more correlated in 2021 than in 2020. Leaf N was more strongly related to pigment indices (i.e., MCARI and CTRI1, Fig. 9b and c) than structural indices (i.e., NDVI and EVI) in both years. These strong relationships were not always consistent over 2 years, as illustrated in Table 3. For example, the chlorophyll index TCARI/OSAVI was unable to capture the existing N variability in 2021 ($r^2 = 0$, n.s.) as it did in 2020 ($r^2 = 0.57$, p-value <0.01).

Some pigment indices in Table 3 stand out in terms of their high correlations with N for both years. For example, MCARI had an r^2 of 0.61 and 0.48 (p-values <0.005, Fig. 9b) in 2020 and 2021, respectively. PRI_{515} (PRI index using reference band at 515 nm to minimize structural effects) (Hernández-Clemente et al., 2011; Stagakis et al., 2012; Zarco-Tejada et al., 2012) was superior to PRI (at 570 nm) in both 2020 and 2021(Fig. 9d).

Table 3
Coefficients of determination (r^2) for the intercorrelations among standard indices at canopy level from the same 15 study plots in two consecutive years and leaf N concentration (%), Dualex-derived leaf chlorophyll content (C_{ab}), nitrogen balance index (NBI), and steady-state chlorophyll fluorescence (Ft) measured with FluorPen.

	N (%)		C_{ab}		NBI		Ft	
	2020	2021	2020	2021	2020	2021	2020	2021
Structural indices								
NDVI	0.25*	0.13	0.49***	0.10	0.07	0.12	0.04	0.05
EVI	0.37**	0.29**	0.56***	0.01	0.14	0.43***	0.07	0.17
MCARI2	0.40**	0.28**	0.58***	0.03	0.16	0.36**	0.09	0.15
RDVI	0.36**	0.25*	0.58***	0.01	0.15	0.36**	0.07	0.13
OSAVI	0.34**	0.22*	0.57***	0.03	0.13	0.29**	0.06	0.10
Chlorophyll a + b indices								
MCARI	0.61***	0.48***	0.54***	0.00	0.55***	0.39**	0.44***	0.31**
TCARI/OSAVI	0.57***	0.00	0.15	0.04	0.46***	0.00	0.48***	0.01
NPQI	0.38**	0.00	0.37**	0.12	0.39**	0.00	0.36**	0.05
PSSRa	0.24*	0.15	0.49***	0.08	0.08	0.16	0.04	0.06
PSSRb	0.14	0.12	0.43***	0.06	0.03	0.14	0.01	0.05
PSSRc	0.23*	0.16	0.58***	0.02	0.12	0.21*	0.02	0.05
SIPI	0.17	0.05	0.37**	0.16	0.02	0.03	0.02	0.02
CTRI1	0.61***	0.52***	0.35**	0.03	0.76***	0.51***	0.45***	0.18
Indices calculated in the green region								
PRI	0.10	0.27**	0.01	0.13	0.24*	0.36**	0.10	0.08
PRI_{515}	0.69***	0.47***	0.61***	0.11	0.43***	0.38**	0.33**	0.25*
PRI•CI	0.13	0.18	0.49***	0.15	0.03	0.21*	0.00	0.05
Fluorescence quantification								
SIF	0.60***	0.55***	0.28**	0.00	0.46***	0.67***	0.73***	0.30**
Canopy temperature								
CWSI	0.05	0.03	0.00	0.23*	0.31**	0.01	0.10	0.03

*p-value <0.1; **p-value <0.05; ***p-value <0.01.
C_{ab}: Chlorophyll $a + b$ content; NBI: Nitrogen Balance Index; Ft: steady-state chlorophyll fluorescence.

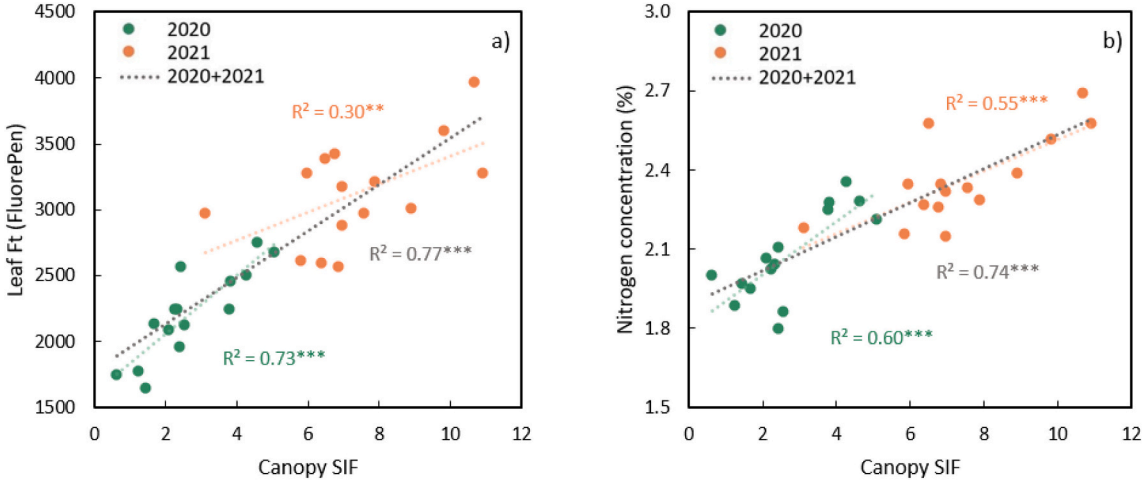

Fig. 8. Relationships between canopy SIF and a) leaf steady-state chlorophyll fluorescence (Ft) and b) leaf N concentration (%) in 2020 (green), 2021 (orange), and the combined years (grey). *p-value <0.5; **p-value <0.05; ***p-value <0.005. (For interpretation of the references to colour in this figure legend, the reader is referred to the web version of this article.)

Many structural and pigment indices showed inconsistent trends across seasons, as shown in Fig. 9 and Table 3. When looking at data from the 2 years combined, no variables from Fig. 9 were significantly correlated with leaf N. NDVI had relatively weak associations with leaf N in each year throughout this heterogeneous orchard. By contrast, airborne SIF calculated from the illuminated crown pixels was consistently related to leaf N across years (Fig. 8). CWSI was not consistently correlated with leaf N or pigment content in either year (Table 3).

3.3. Plant trait retrieval from the FluSAIL radiative transfer model

Modelled reflectance spectra from FluSAIL showed close agreement with observed spectra extracted from pure tree crown vegetation pixels in airborne hyperspectral imagery, yielding average RMSE values of

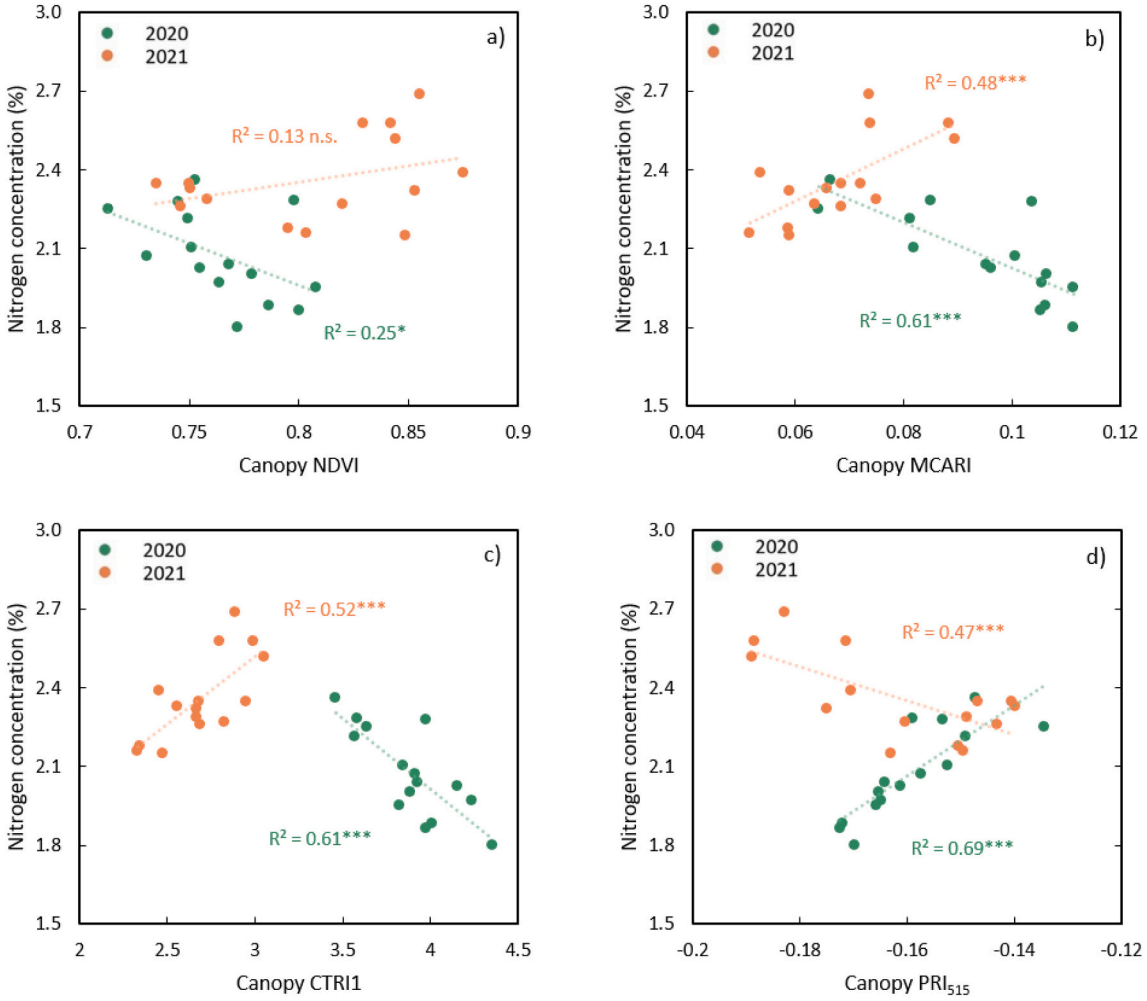

Fig. 9. Leaf N against a) NDVI, b) MCARI, c) CTRI1, and d) PRI_{515} calculated from hyperspectral imagery acquired in 2020 (green) and 2021 (orange). *p-value <0.05; **p-value <0.01; ***p-value <0.005; n.s. = not significant. (For interpretation of the references to colour in this figure legend, the reader is referred to the web version of this article.)

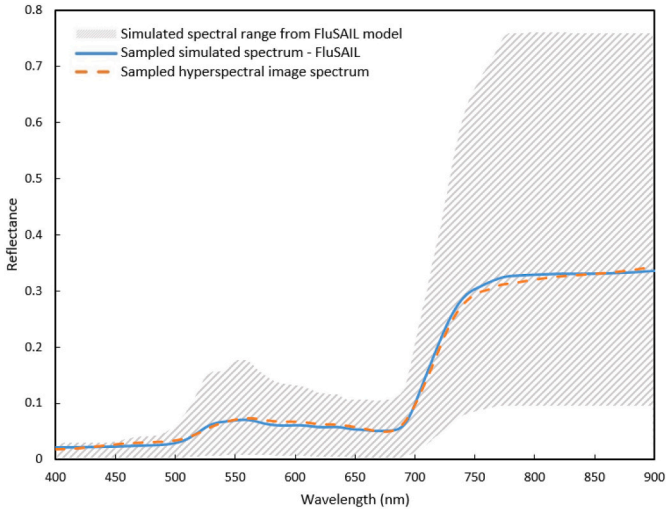

Fig. 10. Comparison of the average hyperspectral image spectrum (orange dashed line) and the corresponding spectrum obtained from the FluSAIL model inversion (blue solid line) for one monitored plot. The simulated FluSAIL spectral range is shown in the shaded grey area. (For interpretation of the references to colour in this figure legend, the reader is referred to the web version of this article.)

0.008 and 0.007 for 2020 and 2021, respectively. Fig. 10 illustrates a simulated and observed spectra as well as a range of simulated spectra from the FluSAIL LUT.

In 2020, leaf C_{ab} from model inversion was strongly correlated to both the Dualex chlorophyll measurement (r^2 = 0.66, p-value <0.001) and leaf N (r^2 = 0.73, p-value <0.001). As with the hyperspectral indices, no model-derived measures were significantly correlated with Dualex chlorophyll in 2021 (Table 4). In addition to C_{ab}, other pigments (i.e., C_{car} and C_x) also presented significant relationships with leaf N.

C_x, which is sensitive to the de-epoxidation state of the xanthophyll cycle, was significantly correlated with canopy PRI_{515} (r^2 = 0.68 and 0.60 in 2020 and 2021, p-values <0.001) and with leaf N (r^2 = 0.61 and 0.62 in 2020 and 2021, p-values <0.001). C_{ab} was also closely related to canopy PRI_{515} (r^2 = 0.80, p-value <0.001) and SIF (r^2 = 0.51, p-value <0.005). No significant relationship was detected between the retrieved LAI and leaf N throughout the orchard across years. These results suggest that pigment content and N were highly correlated with biochemical constituents and SIF but showed little effects on the crown structure.

3.4. *Leaf N status assessment from the airborne-estimated plant traits and SIF*

The final model for leaf N using traits derived from hyperspectral imagery was strongly correlated to field-measured N across years (r^2 = 0.96, p-value <0.001). FluSAIL-inverted C_{ab} and airborne-derived SIF

Table 4
Coefficients of determination (r^2) for correlations among model-derived estimates from the same 15 study plots in two consecutive years, including leaf chlorophyll *a* + *b* (C_{ab}), carotenoids (C_{car}), anthocyanin (Anth), dry matter content (C_{dm}), photochemical reflectance parameter (C_x), leaf area index (LAI), measured leaf N concentration (%), Dualex-measured chlorophyll content, canopy SIF, and canopy photochemical reflectance index (PRI_{515}).

Estimated traits	N (%)		Leaf C_{ab}		Canopy SIF		Canopy PRI_{515}	
	2020	2021	2020	2021	2020	2021	2020	2021
C_{ab} (μg/cm^2)	0.73***	0.66***	0.66***	0.10	0.51**	0.52**	0.80***	0.82***
C_{car} (μg/cm^2)	0.75***	0.56**	0.65***	0.15	0.56**	0.43*	0.72***	0.50**
Anth (μg/cm^2)	0.58***	0.09	0.63***	0.00	0.45*	0.04	0.85***	0.00
C_x	0.61***	0.62***	0.50**	0.01	0.54**	0.57**	0.68***	0.60***
C_{dm} (g/cm^2)	0.36*	0.20	0.58**	0.04	0.20	0.31*	0.59***	0.79***
LAI	0.02	0.05	0.02	0.16	0.07	0.06	0.02	0.49**

*p-value <0.05; **p-value <0.005; ***p-value <0.001.

had the greatest OOB predictor scores, followed by other biochemical constituents (e.g., C_{car} and C_x), as illustrated in Fig. 11a. While the structural trait LAI (p-value >0.1) and the thermal-based water stress indicator CWSI (p-value >0.05) were not statistically significant predictors of N. VIF analysis revealed that C_{ab} and SIF were not collinear, but other biochemical constituents (C_{car}, C_x, and C_{dm}) were discarded from further analysis with a VIF > 5 (empty bars in Fig. 11a). Fig. 11b shows that C_{ab} and SIF were the most important predictors of N for both years, yielding r^2 and RMSE of 0.95 and 0.05%, respectively.

When using combined data from both years, the Gaussian regression model using chlorophyll exclusively as a predictor explained 49% (p-value <0.001) of the variability in N (Fig. 12a) across the almond orchard. A Gaussian process regression model including C_{ab} and SIF considerably increased the performance (r^2 = 0.95, p-value <0.001, RMSE = 0.05%, Fig. 12b). This model with C_{ab} and SIF outperformed any other combination of traits quantified from the hyperspectral imagery for predicting leaf N. As an example, the addition of a structural parameter (LAI) to the model only resulted in a slight increase of 0.02 in r^2 and a 0.01% reduction in RMSE (Fig. 12c) but yielded reasonable results when coupled to SIF (r^2 = 0.81, p-value <0.001, RMSE = 0.1%,

Fig. 11. The relative contribution from OOB importance scores of each variable to the predicted N concentration from a) all plant traits estimated from hyperspectral and thermal imagery and b) a non-collinear subset of variables (VIF < 5).

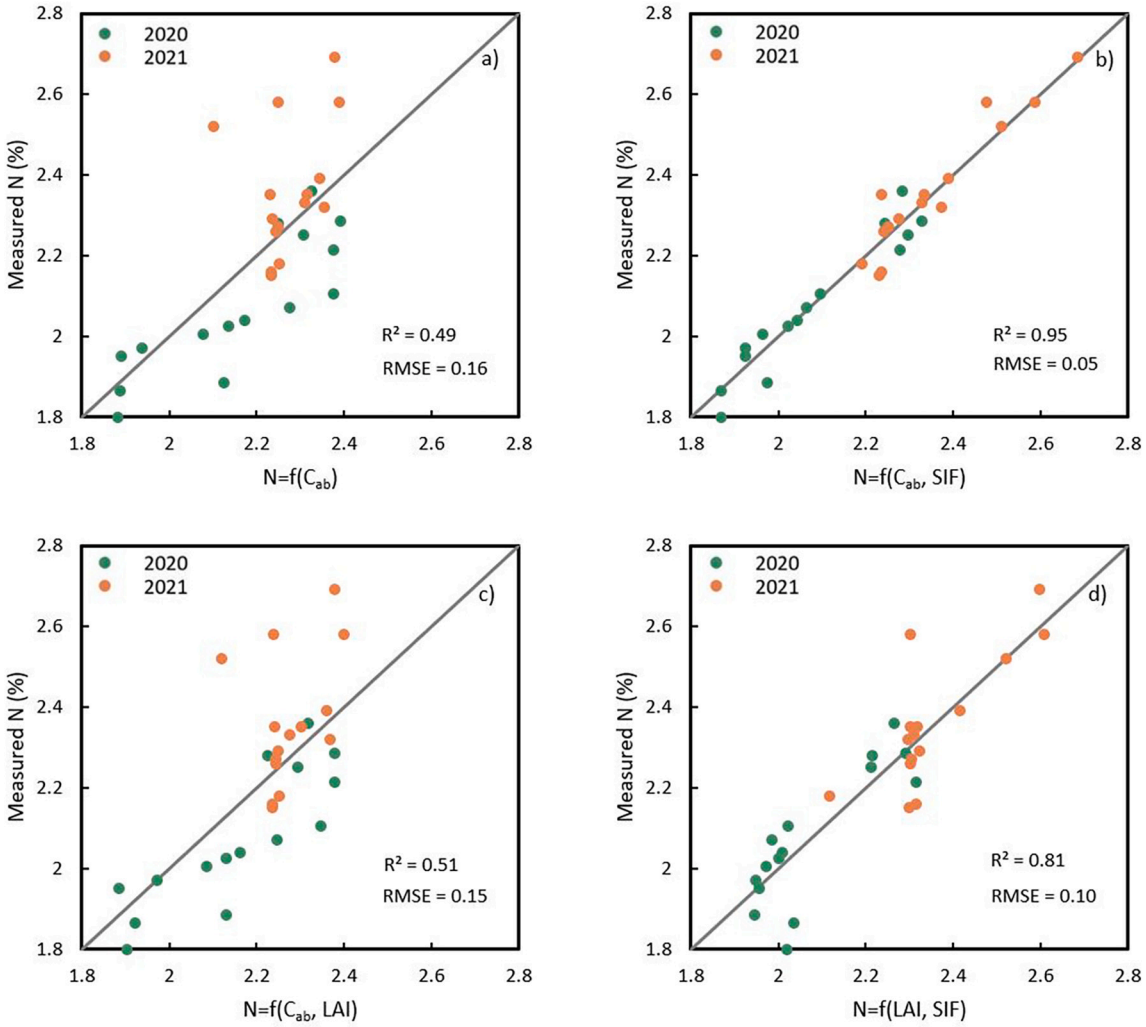

Fig. 12. Correlations between leaf N concentration (%) and predicted N using models based on a) chlorophyll $a + b$ content alone, b) chlorophyll $a + b$ content with canopy SIF, c) chlorophyll $a + b$ content with leaf area index (LAI), and d) LAI with canopy SIF. The grey diagonal line is the 1:1 line. All p-values <0.001.

Fig. 12d). The consistency in the results obtained from the two growing seasons suggests the importance of combining C_{ab} and SIF to assess leaf N status as opposed to standard methods based on individual traits or single vegetation indices, which are generally affected by management practices and the changing growing conditions naturally varying across seasons.

The N prediction map based on a model using C_{ab} and SIF as predictors revealed that tree N was spatially variable across the orchard in 2021 (Fig. 13). As expected, the pattern of N predictions integrates trends in chlorophyll $a + b$ content and SIF.

4. Discussion

Previous studies using RS spectroscopy to estimate leaf N have often focused on developing multispectral indices or proxies from leaf or canopy spectra. These methods usually require the development of empirical models relating leaf N to chlorophyll-sensitive vegetation indices (Clevers and Kooistra, 2011; Fitzgerald et al., 2010; Gabriel et al., 2017; Inoue et al., 2012; Pancorbo et al., 2021; Schlemmer et al., 2013) or combinations of bands and indices (Fitzgerald et al., 2010; Haboudane et al., 2002). However, these methods fail to explain leaf N variability in woody crops that are characterized by structurally complex canopies that are managed to increase productivity. In these highly managed orchard canopies, the relationship between structure and nutrient levels is uncoupled; therefore, structural index-based models are not appropriate (Table 4). In these orchard canopies, the main drivers for the observed structural changes are the planting density and the fractional cover, which add additional complexity to the use of structural RS vegetation indices as indicators of nutrient levels. In these structurally complex orchards, the spectral indices are heavily affected by the canopy architecture and by structural parameters, such as leaf density, which in turn interact with the illumination and observation geometry within the canopy (Broge and Leblanc, 2001; Haboudane et al., 2002; Wang et al., 2018). Therefore, the variability observed with standard vegetation indices such as NDVI and other structurally sensitive indicators may not necessarily represent the nutrient variability, but instead the heterogeneity due to different tree ages, crown densities, and planting grids that usually coexist in large well-managed orchards such as the one used in this study.

The assessment of the physiological status, independent from the structure and canopy architecture using plant traits through RTM model inversion, is particularly beneficial in the case of structurally complex canopies (Malenovský et al., 2013) when trying to capture the within-field spatial variability of the leaf nutrient status independent from the structural variability. In this study, we found that plant physiological estimates derived from RTM inversion using VNIR hyperspectral imagery were generally stronger and more consistent predictors of leaf N status than the empirical models built with vegetation indices. In particular, RTM-retrieved pigment C_{ab} was the strongest predictor (Fig. 11), consistent with the results of Camino et al. (2018a) for wheat.

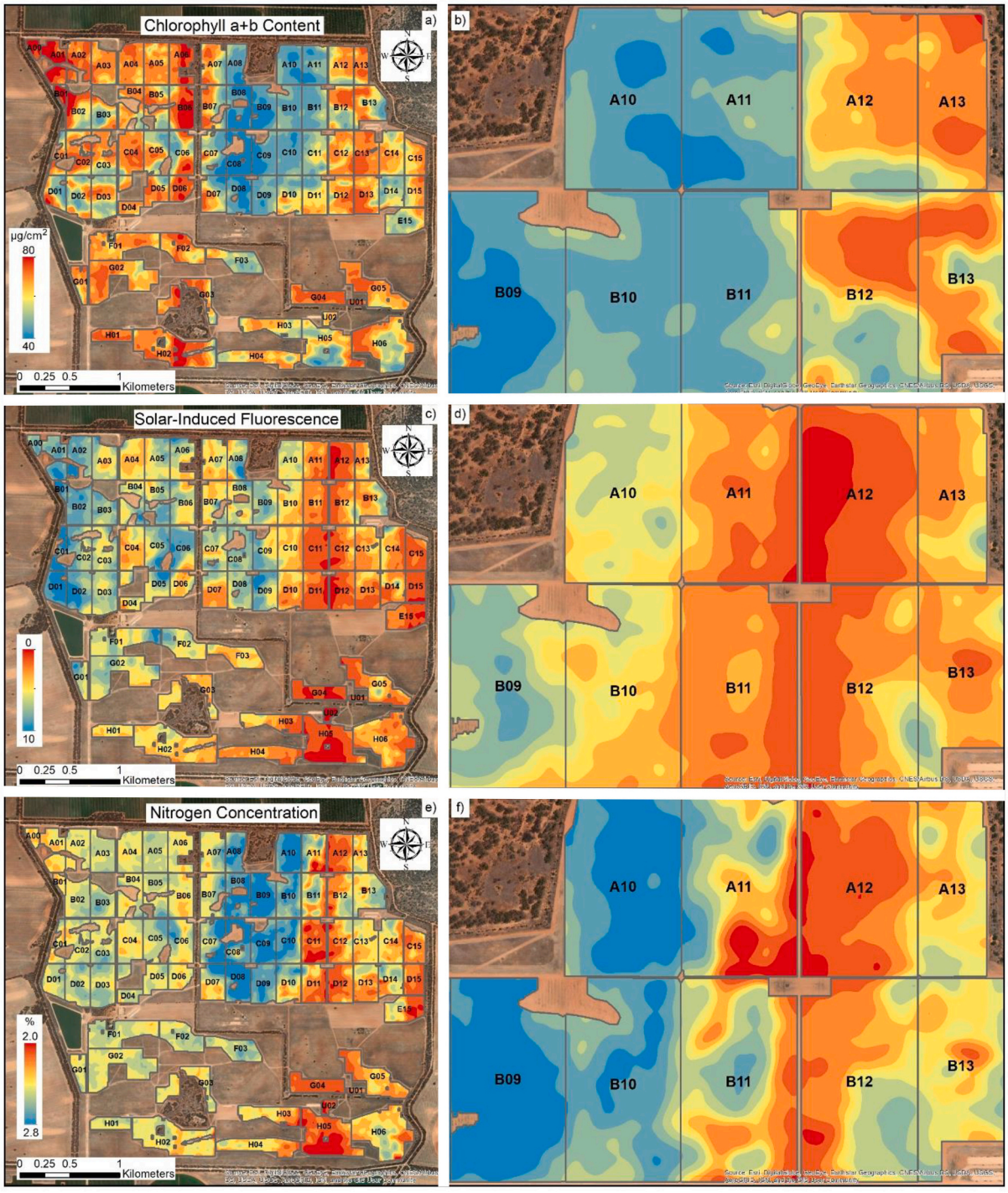

Fig. 13. Interpolated map of a) chlorophyll $a + b$ content, c) solar-induced fluorescence, and e) predicted N concentration derived from C_{ab} and SIF in 2021. Right column contains zoomed-in views (b, d and f) of the scenes on the left in the northeast blocks. Block numbers are displayed in the centers.

RTM-based carotenoid content and the xanthophyll cycle (C_x) parameter were also more strongly related to leaf N than vegetation indices in our study, as both are involved in light-harvesting regulation that is associated with photosynthetic efficiency (Ruban et al., 1999). For instance, RTM-based chlorophyll $a + b$ content was strongly correlated with leaf N for both years of study ($r^2 = 0.73$ in 2020 and 0.66 in 2021, p-values <0.001), whereas the chlorophyll-sensitive index TCARI/OSAVI was not correlated with N in 2021 ($r^2 = 0$, n.s.), suggesting those indices are not reliable indicators for N assessment across seasons. Spectral indices are greatly affected by management practices and background changes across orchards and years, leading to inconsistencies that may make them inappropriate for operational purposes.

The fact that both model-inverted LAI and structural hyperspectral indices were poorly related to leaf N supports the idea that canopy structure is not driven by nutrient availability in well-managed intensive orchards. As a consequence, it is not surprising that the widely used structural index NDVI was inadequate for predicting leaf N in this context. Ground-based leaf chlorophyll measurements were poorly related to leaf N when leaf N was high in 2021. This is consistent with the results of Jifon et al. (2005), who found the relationship between

chlorophyll meter readings and leaf N was stronger at low chlorophyll concentrations than at higher chlorophyll concentrations. At high N concentrations, there is a possibility that some N may be allocated to soluble protein rather than pigment-protein complexes (Evans, 1989). And the soluble protein and pigment complexes in leaves can be imbalanced depending on leaf physical characteristics, plant age, environmental factors, and management practices (Bondada and Syvertsen, 2003; Evans and Poorter, 2001; Syvertsen et al., 1995; Syvertsen, 1984). In our study, leaf nitrogen balance index was more strongly correlated with leaf N and canopy indices as it incorporated the ratio of a second pigment flavonoid into the calculation. This phenomenon was also observed at the canopy level for both chlorophyll-sensitive vegetation indices and RTM-based pigment concentrations. C_{ab} at the canopy level was more strongly related to leaf N than C_{ab} at the leaf level, which may be attributed to the fact that the field-collected leaf measurements came from lower layers of the tree crown, whereas the imagery captured the upper layers. Our results provide evidence that RTM-based leaf physiological traits provide additional benefits over standard structural indices for assessing leaf N in orchards, particularly when multiple varieties, ages, and management practices coexist within the orchard.

Several studies have shown that SIF derived from sub-meter narrowband imagery, in which the depth of the oxygen absorption feature can be quantified, is an effective tool for detecting plant stress in precision agriculture (Calderón et al., 2013; Camino et al., 2018a; Camino et al., 2018b; Quemada et al., 2014; Raya-Sereno et al., 2021; Zarco-Tejada et al., 2012). In this study, we also found a strong association between fluorescence and leaf N, consistent with the literature (Cendrero-Mateo et al., 2016; Corp et al., 2003; Schächtl et al., 2005), yielding $r^2 = 0.74$ (p-value <0.005) over the course of 2 years at both leaf and canopy levels. Airborne-quantified SIF was the second most important predictor of leaf N after C_{ab} and outperformed any other vegetation index or structural and temperature-based plant traits in terms of correlation and consistency across years. When combined with RTM-based traits, SIF significantly improved model performance for predicting leaf N. The model that included C_{ab} and SIF explained 95% of the leaf N variability (p-value <0.001), improving upon results obtained with C_{ab} alone ($r^2 = 0.49$, p-value <0.001) accounting for different plant varieties, ages, planting patterns, water status levels, and fertilizer management practices across 2 years.

CWSI, a thermal canopy water status index, was poorly associated with leaf N and relatively inconsistent across years. Overall, we found no evidence of a relationship between CWSI and leaf N, suggesting that leaf N variability was not driven by water status in this well-managed intensive almond orchard.

5. Conclusions

This study demonstrates that leaf N estimation conducted in an almond orchard across 2 years was significantly improved when SIF was included alongside RTM-based leaf chlorophyll $a + b$ content. Among all spectral plant traits evaluated from hyperspectral imagery, including all RTM-derived leaf biochemical constituents, SIF, and structural and water stress traits, the retrieved leaf chlorophyll $a + b$ and SIF were the two most important predictors to explain leaf N variability. The model that incorporated both chlorophyll $a + b$ content and SIF traits explained 95% of the variability in leaf N (p-value <0.001) consistently across 2 years of airborne hyperspectral data collection. Together, these results provide important insights into the quantification of leaf N content in well-managed structurally complex canopies, such as discontinuous tree orchards, demonstrating that traditional vegetation indices and individual plant traits do not sufficiently track leaf N content over well-managed intensive crops typically reaching high N levels.

Credit author statement

Y.W., L.S. and P.J.Z.-T. designed the objectives of this study and designed research; L.S. and P.J.Z.-T supervised the work; Y.W., L.S., and T.P. carried out field work and airborne data collections; Y.W. analysed data and performed research; Y.W. wrote the paper, and L.S., T.P., V.G.-D., D.R. and P.J.Z.-T. contributed and provided comments. All authors read and approved the final submission.

Declaration of Competing Interest

The authors declare that they have no known competing financial interests or personal relationships that could have appeared to influence the work reported in this paper.

Acknowledgment

The authors gratefully acknowledge McPherson Family and Invergowrie Foundation for the financial support and the assistant from the Mallee Regional Innovation Centre (MRIC). Special thanks to Xiaojin Qian from HyperSens Remote Sensing Laboratory for her support in the field, also extend to Rafael Romero, David Notario and Alberto Hornero from QuantaLab IAS-CSIC (Spain) for their contributions in the laboratory. And Brian Slater for allowing this research to be carried out in the Aroona Farms.

References

Abràmoff, M.D., Magalhães, P.J., Ram, S.J., 2004. Image processing with ImageJ. Biophoton. Int. 11 (7), 36–42.
Akinwande, M.O., Dikko, H.G., Samson, A., 2015. Variance inflation factor: as a condition for the inclusion of suppressor variable (s) in regression analysis. Open J. Stat. 5 (07), 754.
Asai, W., Micke, W., Kester, D., Rough, D., 1996. The Evaluation and Selection of Current Varieties; Almond Production Manual, University of California (System). Division of Agriculture and Natural Resources. ANR Publications, California.
Ashraf, M., Harris, P.J., 2013. Photosynthesis under stressful environments: an overview. Photosynthetica 51 (2), 163–190.
Baret, F., Houlès, V., Guerif, M., 2007. Quantification of plant stress using remote sensing observations and crop models: the case of nitrogen management. J. Exp. Bot. 58 (4), 869–880.
Barnes, J.D., Balaguer, L., Manrique, E., Elvira, S., Davison, A., 1992. A reappraisal of the use of DMSO for the extraction and determination of chlorophylls a and b in lichens and higher plants. Environ. Exp. Bot. 32 (2), 85–100.
Bellvert, J., Adeline, K., Baram, S., Pierce, L., Sanden, B.L., Smart, D.R., 2018. Monitoring crop evapotranspiration and crop coefficients over an almond and pistachio orchard throughout remote sensing. Remote Sens. 10 (12), 2001.
Belwalkar, A., Poblete, T., Longmire, A., Hornero, A., Zarco-Tejada, P., 2021. Comparing the retrieval of chlorophyll fluorescence from two airborne hyperspectral imagers with different spectral resolutions for plant phenotyping studies. In: Paper presented at the 2021 IEEE International Geoscience and Remote Sensing Symposium IGARSS.
Belwalkar, A., Poblete, T., Longmire, A., Hornero, A., Hernandez-Clemente, R., Zarco-Tejada, P., 2022. Evaluation of SIF retrievals from narrow-band and sub-nanometer airborne hyperspectral imagers flown in tandem: modelling and validation in the context of plant phenotyping. Remote Sens. Environ. 273 (112986).
Biswal, B., Joshi, P., Raval, M., Biswal, U., 2011. Photosynthesis, a global sensor of environmental stress in green plants: stress signalling and adaptation. Curr. Sci. 47–56.
Blackburn, G.A., 1998. Spectral indices for estimating photosynthetic pigment concentrations: a test using senescent tree leaves. Int. J. Remote Sens. 19 (4), 657–675.
Bondada, B.R., Syvertsen, J.P., 2003. Leaf chlorophyll, net gas exchange and chloroplast ultrastructure in citrus leaves of different nitrogen status. Tree Physiol. 23 (8), 553–559.
Breiman, L., 2001. Random forests. Mach. Learn. 45 (1), 5–32.
Broge, N.H., Leblanc, E., 2001. Comparing prediction power and stability of broadband and hyperspectral vegetation indices for estimation of green leaf area index and canopy chlorophyll density. Remote Sens. Environ. 76 (2), 156–172.
Buckee, G., 1994. Determination of total nitrogen in barley, malt and beer by Kjeldahl procedures and the dumas combustion methodcollaborative trial. J. Inst. Brew. 100 (2), 57–64.
Bullock, D., Anderson, D., 1998. Evaluation of the Minolta SPAD-502 chlorophyll meter for nitrogen management in corn. J. Plant Nutr. 21 (4), 741–755.
Calderón, R., Navas-Cortés, J.A., Lucena, C., Zarco-Tejada, P.J., 2013. High-resolution airborne hyperspectral and thermal imagery for early detection of Verticillium wilt of olive using fluorescence, temperature and narrow-band spectral indices. Remote Sens. Environ. 139, 231–245.
Camino, C., González-Dugo, V., Hernández, P., Sillero, J., Zarco-Tejada, P.J., 2018a. Improved nitrogen retrievals with airborne-derived fluorescence and plant traits quantified from VNIR-SWIR hyperspectral imagery in the context of precision agriculture. Int. J. Appl. Earth Obs. Geoinf. 70, 105–117.

Camino, C., Zarco-Tejada, P.J., Gonzalez-Dugo, V., 2018b. Effects of heterogeneity within tree crowns on airborne-quantified SIF and the CWSI as indicators of water stress in the context of precision agriculture. Remote Sens. 10 (4), 604.
Carter, G.A., 1994. Ratios of leaf reflectances in narrow wavebands as indicators of plant stress. Int. J. Remote Sens. 15 (3), 697–703.
Cendrero-Mateo, M.P., Moran, M.S., Papuga, S.A., Thorp, K., Alonso, L., Moreno, J., Wang, G., 2016. Plant chlorophyll fluorescence: active and passive measurements at canopy and leaf scales with different nitrogen treatments. J. Exp. Bot. 67 (1), 275–286.
Cerovic, Z.G., Masdoumier, G., Ghozlen, N.B., Latouche, G., 2012. A new optical leaf-clip meter for simultaneous non-destructive assessment of leaf chlorophyll and epidermal flavonoids. Physiol. Plant. 146 (3), 251–260.
Cerovic, Z.G., Ghozlen, N.B., Milhade, C., Obert, M., Debuisson, S.B., Moigne, M.L., 2015. Nondestructive diagnostic test for nitrogen nutrition of grapevine (Vitis vinifera L.) based on dualex leaf-clip measurements in the field. J. Agric. Food Chem. 63 (14), 3669–3680.
Chang, S.X., Robison, D.J., 2003. Nondestructive and rapid estimation of hardwood foliar nitrogen status using the SPAD-502 chlorophyll meter. For. Ecol. Manag. 181 (3), 331–338.
Chapman, S.C., Barreto, H.J., 1997. Using a chlorophyll meter to estimate specific leaf nitrogen of tropical maize during vegetative growth. Agron. J. 89 (4), 557–562.
Cheng, L., 2003. Xanthophyll cycle pool size and composition in relation to the nitrogen content of apple leaves. J. Exp. Bot. 54 (381), 385–393.
Clevers, J.G., Gitelson, A.A., 2013. Remote estimation of crop and grass chlorophyll and nitrogen content using red-edge bands on Sentinel-2 and-3. Int. J. Appl. Earth Obs. Geoinf. 23, 344–351.
Clevers, J.G., Kooistra, L., 2011. Using hyperspectral remote sensing data for retrieving canopy chlorophyll and nitrogen content. IEEE J. Sel. Top. Appl. Earth Obs. Remote Sens. 5 (2), 574–583.
Combal, B., Baret, F., Weiss, M., Trubuil, A., Mace, D., Pragnere, A., Wang, L., 2003. Retrieval of canopy biophysical variables from bidirectional reflectance: using prior information to solve the ill-posed inverse problem. Remote Sens. Environ. 84 (1), 1–15.
Conant, R.T., Berdanier, A.B., Grace, P.R., 2013. Patterns and trends in nitrogen use and nitrogen recovery efficiency in world agriculture. Glob. Biogeochem. Cycles 27 (2), 558–566.
Corp, L.A., McMurtrey, J.E., Middleton, E.M., Mulchi, C.L., Chappelle, E.W., Daughtry, C. S., 2003. Fluorescence sensing systems: in vivo detection of biophysical variations in field corn due to nitrogen supply. Remote Sens. Environ. 86 (4), 470–479.
Cummings, C., Miao, Y., Paiao, G.D., Kang, S., Fernández, F.G., 2021. Corn nitrogen status diagnosis with an innovative multi-parameter crop circle phenom sensing system. Remote Sens. 13 (3), 401.
Daughtry, C.S., Walthall, C., Kim, M., De Colstoun, E.B., McMurtrey Iii, J., 2000. Estimating corn leaf chlorophyll concentration from leaf and canopy reflectance. Remote Sens. Environ. 74 (2), 229–239.
Demmig, B., Winter, K., Krüger, A., Czygan, F.-C., 1987. Photoinhibition and zeaxanthin formation in intact leaves: a possible role of the xanthophyll cycle in the dissipation of excess light energy. Plant Physiol. 84 (2), 218–224.
Dong, R., Miao, Y., Wang, X., Chen, Z., Yuan, F., Zhang, W., Li, H., 2020. Estimating plant nitrogen concentration of maize using a leaf fluorescence sensor across growth stages. Remote Sens. 12 (7), 1139.
Dumas, J.B.A., 1831. Procedes de l'analyse organic. Ann. Chim. Phys. 247, 198–213.
Etheridge, R., Pesti, G., Foster, E., 1998. A comparison of nitrogen values obtained utilizing the Kjeldahl nitrogen and Dumas combustion methodologies (Leco CNS 2000) on samples typical of an animal nutrition analytical laboratory. Anim. Feed Sci. Technol. 73 (1–2), 21–28.
Evans, J., 1989. Photosynthesis and nitrogen relationships in leaves of C 3 plants. Oecologia 78 (1), 9–19.
Evans, J., Poorter, H., 2001. Photosynthetic acclimation of plants to growth irradiance: the relative importance of specific leaf area and nitrogen partitioning in maximizing carbon gain. Plant Cell Environ. 24 (8), 755–767.
Filella, I., Serrano, L., Serra, J., Penuelas, J., 1995. Evaluating wheat nitrogen status with canopy reflectance indices and discriminant analysis. Crop Sci. 35 (5), 1400–1405.
Fitzgerald, G., Rodriguez, D., Christensen, L., Belford, R., Sadras, V., Clarke, T., 2006. Spectral and thermal sensing for nitrogen and water status in rainfed and irrigated wheat environments. Precis. Agric. 7 (4), 233–248.
Fitzgerald, G., Rodriguez, D., O'Leary, G., 2010. Measuring and predicting canopy nitrogen nutrition in wheat using a spectral index—the canopy chlorophyll content index (CCCI). Field Crop Res. 116 (3), 318–324.
Flowers, M., Weisz, R., Heiniger, R., 2003. Quantitative approaches for using color infrared photography for assessing in-season nitrogen status in winter wheat. Agron. J. 95 (5), 1189–1200.
Gabriel, J.L., Zarco-Tejada, P.J., López-Herrera, P.J., Pérez-Martín, E., Alonso-Ayuso, M., Quemada, M., 2017. Airborne and ground level sensors for monitoring nitrogen status in a maize crop. Biosyst. Eng. 160, 124–133.
Gamon, J., Penuelas, J., Field, C., 1992. A narrow-waveband spectral index that tracks diurnal changes in photosynthetic efficiency. Remote Sens. Environ. 41 (1), 35–44.
Gareth, J., Daniela, W., Trevor, H., Robert, T., 2013. An Introduction to Statistical Learning: With Applications in R. Spinger.
Garrity, S.R., Eitel, J.U., Vierling, L.A., 2011. Disentangling the relationships between plant pigments and the photochemical reflectance index reveals a new approach for remote estimation of carotenoid content. Remote Sens. Environ. 115 (2), 628–635.
Genty, B., Briantais, J.-M., Baker, N.R., 1989. The relationship between the quantum yield of photosynthetic electron transport and quenching of chlorophyll fluorescence. Biochim. Biophys. Acta 990 (1), 87–92.
Gilmore, A.M., 1997. Mechanistic aspects of xanthophyll cycle-dependent photoprotection in higher plant chloroplasts and leaves. Physiol. Plant. 99 (1), 197–209.
Gitelson, A.A., Merzlyak, M.N., Lichtenthaler, H.K., 1996. Detection of red edge position and chlorophyll content by reflectance measurements near 700 nm. J. Plant Physiol. 148 (3–4), 501–508.
Gitelson, A.A., Gritz, Y., Merzlyak, M.N., 2003. Relationships between leaf chlorophyll content and spectral reflectance and algorithms for non-destructive chlorophyll assessment in higher plant leaves. J. Plant Physiol. 160 (3), 271–282.
Gnyp, M.L., Miao, Y., Yuan, F., Ustin, S.L., Yu, K., Yao, Y., Bareth, G., 2014. Hyperspectral canopy sensing of paddy rice aboveground biomass at different growth stages. Field Crop Res. 155, 42–55.
Gueymard, C.A., 1995. SMARTS2: A simple model of the atmospheric radiative transfer of sunshine. In: Algorithms and Performance Assessment. Florida Solar Energy Center Cocoa, FL.
Gueymard, C.A., 2001. Parameterized transmittance model for direct beam and circumsolar spectral irradiance. Sol. Energy 71 (5), 325–346.
Gueymard, C.A., Myers, D., Emery, K., 2002. Proposed reference irradiance spectra for solar energy systems testing. Sol. Energy 73 (6), 443–467.
Haboudane, D., Miller, J.R., Tremblay, N., Zarco-Tejada, P.J., Dextraze, L., 2002. Integrated narrow-band vegetation indices for prediction of crop chlorophyll content for application to precision agriculture. Remote Sens. Environ. 81 (2–3), 416–426.
Haboudane, D., Miller, J.R., Pattey, E., Zarco-Tejada, P.J., Strachan, I.B., 2004. Hyperspectral vegetation indices and novel algorithms for predicting green LAI of crop canopies: modeling and validation in the context of precision agriculture. Remote Sens. Environ. 90 (3), 337–352.
Hassoun, M.H., 1995. Fundamentals of Artificial Neural Networks. MIT press.
Hernández-Clemente, R., Navarro-Cerrillo, R.M., Suárez, L., Morales, F., Zarco-Tejada, P. J., 2011. Assessing structural effects on PRI for stress detection in conifer forests. Remote Sens. Environ. 115 (9), 2360–2375.
Hill, S., Stephenson, D., Taylor, B., 1985. Almond pollination studies: pollen production and viability, flower emergence and cross-pollination tests. Aust. J. Exp. Agric. 25 (3), 697–704.
Huang, Z.-A., Jiang, D.-A., Yang, Y., Sun, J.-W., Jin, S.-H., 2004. Effects of nitrogen deficiency on gas exchange, chlorophyll fluorescence, and antioxidant enzymes in leaves of rice plants. Photosynthetica 42 (3), 357–364.
Idso, S., Jackson, R., Pinter Jr., P., Reginato, R., Hatfield, J., 1981. Normalizing the stress-degree-day parameter for environmental variability. Agric. Meteorol. 24, 45–55.
Inoue, Y., Sakaiya, E., Zhu, Y., Takahashi, W., 2012. Diagnostic mapping of canopy nitrogen content in rice based on hyperspectral measurements. Remote Sens. Environ. 126, 210–221.
Jackson, R.D., Idso, S., Reginato, R., Pinter Jr., P., 1981. Canopy temperature as a crop water stress indicator. Water Resour. Res. 17 (4), 1133–1138.
Jacquemoud, S., Verhoef, W., Baret, F., Bacour, C., Zarco-Tejada, P.J., Asner, G.P., Ustin, S.L., 2009. PROSPECT+ SAIL models: a review of use for vegetation characterization. Remote Sens. Environ. 113, S56–S66.
Jifon, J.L., Syvertsen, J.P., Whaley, E., 2005. Growth environment and leaf anatomy affect nondestructive estimates of chlorophyll and nitrogen in Citrus sp. leaves. J. Am. Soc. Hortic. Sci. 130 (2), 152–158.
Jongschaap, R.E., Booij, R., 2004. Spectral measurements at different spatial scales in potato: relating leaf, plant and canopy nitrogen status. Int. J. Appl. Earth Obs. Geoinf. 5 (3), 205–218.
Kimes, D.S., Knyazikhin, Y., Privette, J., Abuelgasim, A., Gao, F., 2000. Inversion methods for physically-based models. Remote Sens. Rev. 18 (2–4), 381–439.
Kjeldahl, J., 1883. A new method for the estimation of nitrogen in organic compounds. Z. Anal. Chem. 22 (1), 366.
Krause, G., Weis, E., 1991. Chlorophyll fluorescence and photosynthesis: the basics. Annu. Rev. Plant Biol. 42 (1), 313–349.
Li, F., Miao, Y., Feng, G., Yuan, F., Yue, S., Gao, X., Chen, X., 2014. Improving estimation of summer maize nitrogen status with red edge-based spectral vegetation indices. Field Crop Res. 157, 111–123.
Li, H., Zhang, Y., Lei, Y., Antoniuk, V., Hu, C., 2020. Evaluating different non-destructive estimation methods for winter wheat (Triticum aestivum L.) nitrogen status based on canopy spectrum. Remote Sens. 12 (1), 95.
Liu, H.Q., Huete, A., 1995. A feedback based modification of the NDVI to minimize canopy background and atmospheric noise. IEEE Trans. Geosci. Remote Sens. 33 (2), 457–465.
Lu, C., Zhang, J., 2000. Photosynthetic CO2 assimilation, chlorophyll fluorescence and photoinhibition as affected by nitrogen deficiency in maize plants. Plant Sci. 151 (2), 135–143.
Maier, S.W., Günther, K.P., Stellmes, M., 2004. Sun-induced fluorescence: a new tool for precision farming. Digit. Imaging Spect. Tech. 66, 207–222.
Malenovský, Z., Homolová, L., Zurita-Milla, R., Lukeš, P., Kaplan, V., Hanuš, J., Schaepman, M.E., 2013. Retrieval of spruce leaf chlorophyll content from airborne image data using continuum removal and radiative transfer. Remote Sens. Environ. 131, 85–102.
Manna, M., Swarup, A., Wanjari, R., Ravankar, H., Mishra, B., Saha, M., Sarap, P., 2005. Long-term effect of fertilizer and manure application on soil organic carbon storage, soil quality and yield sustainability under sub-humid and semi-arid tropical India. Field Crop Res. 93 (2–3), 264–280.
Matson, P.A., Naylor, R., Ortiz-Monasterio, I., 1998. Integration of environmental, agronomic, and economic aspects of fertilizer management. Science 280 (5360), 112–115.
Matsushita, B., Yang, W., Chen, J., Onda, Y., Qiu, G., 2007. Sensitivity of the enhanced vegetation index (EVI) and normalized difference vegetation index (NDVI) to

topographic effects: a case study in high-density cypress forest. sensors 7 (11), 2636–2651.
Maxwell, K., Johnson, G.N., 2000. Chlorophyll fluorescence—a practical guide. J. Exp. Bot. 51 (345), 659–668.
Middleton, E.M., Huemmrich, K.F., Cheng, Y.-B., Margolis, H.A., 2016. 12 Spectral bioindicators of photosynthetic efficiency and vegetation stress. In: Hyperspectral Remote Sensing of Vegetation. CRC Press, pp. 265–288.
Mohammed, G.H., Binder, W., Gillies, S., 1995. Chlorophyll fluorescence: a review of its practical forestry applications and instrumentation. Scand. J. For. Res. 10 (1–4), 383–410.
Mohammed, G.H., Colombo, R., Middleton, E.M., Rascher, U., van der Tol, C., Nedbal, L., Meroni, M., 2019. Remote sensing of solar-induced chlorophyll fluorescence (SIF) in vegetation: 50 years of progress. Remote Sens. Environ. 231, 111177.
Murchie, E.H., Lawson, T., 2013. Chlorophyll fluorescence analysis: a guide to good practice and understanding some new applications. J. Exp. Bot. 64 (13), 3983–3998.
Nageswara Rao, R., Talwar, H., Wright, G., 2001. Rapid assessment of specific leaf area and leaf nitrogen in peanut (Arachis hypogaea L.) using a chlorophyll meter. J. Agron. Crop Sci. 186 (3), 175–182.
Nguy-Robertson, A., Gitelson, A., Peng, Y., Viña, A., Arkebauer, T., Rundquist, D., 2012. Green leaf area index estimation in maize and soybean: combining vegetation indices to achieve maximal sensitivity. Agron. J. 104 (5), 1336–1347.
Niblack, W., 1985. An Introduction to Digital Image Processing. Strandberg Publishing Company.
Nigon, T.J., Yang, C., Dias Paiao, G., Mulla, D.J., Knight, J.F., Fernández, F.G., 2020. Prediction of early season nitrogen uptake in maize using high-resolution aerial hyperspectral imagery. Remote Sens. 12 (8), 1234.
Niyogi, K.K., Björkman, O., Grossman, A.R., 1997. The roles of specific xanthophylls in photoprotection. Proc. Natl. Acad. Sci. 94 (25), 14162–14167.
O'brien, R.M., 2007. A caution regarding rules of thumb for variance inflation factors. Qual. Quant. 41 (5), 673–690.
Padilla, F.M., de Souza, R., Peña-Fleitas, M.T., Gallardo, M., Gimenez, C., Thompson, R. B., 2018. Different responses of various chlorophyll meters to increasing nitrogen supply in sweet pepper. Front. Plant Sci. 9, 1752.
Pancorbo, J., Camino, C., Alonso-Ayuso, M., Raya-Sereno, M., Gonzalez-Fernandez, I., Gabriel, J., Quemada, M., 2021. Simultaneous assessment of nitrogen and water status in winter wheat using hyperspectral and thermal sensors. Eur. J. Agron. 127, 126287.
Panhwar, Q.A., Ali, A., Naher, U.A., Memon, M.Y., 2019. Fertilizer management strategies for enhancing nutrient use efficiency and sustainable wheat production. In: Organic Farming. Elsevier, pp. 17–39.
Penuelas, J., Baret, F., Filella, I., 1995. Semi-empirical indices to assess carotenoids/chlorophyll a ratio from leaf spectral reflectance. Photosynthetica 31 (2), 221–230.
Perry, E.M., Fitzgerald, G.J., Nuttall, J.G., O'Leary, G.J., Schulthess, U., Whitlock, A., 2012. Rapid estimation of canopy nitrogen of cereal crops at paddock scale using a canopy chlorophyll content index. Field Crop Res. 134, 158–164.
Phansalkar, N., More, S., Sabale, A., Joshi, M., 2011. Adaptive local thresholding for detection of nuclei in diversity stained cytology images. In: Paper Presented at the 2011 International Conference on Communications and Signal Processing.
Pinter Jr., P.J., Hatfield, J.L., Schepers, J.S., Barnes, E.M., Moran, M.S., Daughtry, C.S., Upchurch, D.R., 2003. Remote sensing for crop management. Photogramm. Eng. Remote. Sens. 69 (6), 647–664.
Plascyk, J.A., Gabriel, F.C., 1975. The Fraunhofer line discriminator MKII-an airborne instrument for precise and standardized ecological luminescence measurement. IEEE Trans. Instrum. Meas. 24 (4), 306–313.
Porcar-Castell, A., Tyystjärvi, E., Atherton, J., Van der Tol, C., Flexas, J., Pfündel, E.E., Berry, J.A., 2014. Linking chlorophyll a fluorescence to photosynthesis for remote sensing applications: mechanisms and challenges. J. Exp. Bot. 65 (15), 4065–4095.
Quemada, M., Gabriel, J.L., Zarco-Tejada, P., 2014. Airborne hyperspectral images and ground-level optical sensors as assessment tools for maize nitrogen fertilization. Remote Sens. 6 (4), 2940–2962.
Ramalho, J.C., Pons, T.L., Groeneveld, H.W., Azinheira, H.G., Nunes, M.A., 2000. Photosynthetic acclimation to high light conditions in mature leaves of Coffea arabica L.: role of xanthophylls, quenching mechanisms and nitrogen nutrition. Funct. Plant Biol. 27 (1), 43–51.
Raya-Sereno, M.D., Alonso-Ayuso, M., Pancorbo, J.L., Gabriel, J.L., Camino, C., Zarco-Tejada, P.J., Quemada, M., 2021. Residual effect and N fertilizer rate detection by high-resolution VNIR-SWIR hyperspectral imagery and solar-induced chlorophyll fluorescence in wheat. IEEE Trans. Geosci. Remote Sens. 60, 1–17.
Romina, D.S., Teresa, P.-F., Rodney, B.T., Marisa, G., Rafael, G., Francisco, M.P., 2019. The use of chlorophyll meters to assess crop N status and derivation of sufficiency values for sweet pepper. Sensors 19 (13), 2949.
Rondeaux, G., Steven, M., Baret, F., 1996. Optimization of soil-adjusted vegetation indices. Remote Sens. Environ. 55 (2), 95–107.
Roujean, J.-L., Breon, F.-M., 1995. Estimating PAR absorbed by vegetation from bidirectional reflectance measurements. Remote Sens. Environ. 51 (3), 375–384.
Rouse, J.W., Haas, R.H., Schell, J.A., Deering, D.W., 1974. Monitoring vegetation systems in the Great Plains with ERTS. NASA Spec. Publ. 351 (1974), 309.
Ruban, A.V., Lee, P.J., Wentworth, M., Young, A.J., Horton, P., 1999. Determination of the stoichiometry and strength of binding of xanthophylls to the photosystem II light harvesting complexes. J. Biol. Chem. 274 (15), 10458–10465.
Saibo, N.J., Lourenço, T., Oliveira, M.M., 2009. Transcription factors and regulation of photosynthetic and related metabolism under environmental stresses. Ann. Bot. 103 (4), 609–623.
Sayed, O., 2003. Chlorophyll fluorescence as a tool in cereal crop research. Photosynthetica 41 (3), 321–330.
Schächtl, J., Huber, G., Maidl, F.-X., Sticksel, E., Schulz, J., Haschberger, P., 2005. Laser-induced chlorophyll fluorescence measurements for detecting the nitrogen status of wheat (Triticum aestivum L.) canopies. Precis. Agric. 6 (2), 143–156.
Schepers, J., Francis, D., Vigil, M., Below, F., 1992. Comparison of corn leaf nitrogen concentration and chlorophyll meter readings. Commun. Soil Sci. Plant Anal. 23 (17–20), 2173–2187.
Schlemmer, M., Gitelson, A., Schepers, J., Ferguson, R., Peng, Y., Shanahan, J., Rundquist, D., 2013. Remote estimation of nitrogen and chlorophyll contents in maize at leaf and canopy levels. Int. J. Appl. Earth Obs. Geoinf. 25, 47–54.
Shcherbak, I., Millar, N., Robertson, G.P., 2014. Global metaanalysis of the nonlinear response of soil nitrous oxide (N2O) emissions to fertilizer nitrogen. Proc. Natl. Acad. Sci. 111 (25), 9199–9204.
Snyder, C.S., Bruulsema, T.W., Jensen, T.L., Fixen, P.E., 2009. Review of greenhouse gas emissions from crop production systems and fertilizer management effects. Agric. Ecosyst. Environ. 133 (3–4), 247–266.
Stagakis, S., González-Dugo, V., Cid, P., Guillén-Climent, M.L., Zarco-Tejada, P.J., 2012. Monitoring water stress and fruit quality in an orange orchard under regulated deficit irrigation using narrow-band structural and physiological remote sensing indices. ISPRS J. Photogramm. Remote Sens. 71, 47–61.
Stevenson, F.J., Cole, M.A., 1999. Cycles of Soils: Carbon, Nitrogen, Phosphorus, Sulfur, Micronutrients. John Wiley & Sons.
Syvertsen, J.P., 1984. Light acclimation in citrus leaves. I: changes in physical characteristics, chlorophyll, and nitrogen content. J. Am. Soc. Hortic. Sci. 109 (6), 807–812.
Syvertsen, J., Lloyd, J., McConchie, C., Kriedemann, P., Farquhar, G., 1995. On the relationship between leaf anatomy and CO2 diffusion through the mesophyll of hypostomatous leaves. Plant Cell Environ. 18 (2), 149–157.
Thorp, K., Wang, G., West, A., Moran, M., Bronson, K., White, J., Mon, J., 2012. Estimating crop biophysical properties from remote sensing data by inverting linked radiative transfer and ecophysiological models. Remote Sens. Environ. 124, 224–233.
Tóth, V.R., Mészáros, I., Veres, S., Nagy, J., 2002. Effects of the available nitrogen on the photosynthetic activity and xanthophyll cycle pool of maize in field. J. Plant Physiol. 159 (6), 627–634.
Verhoef, W., 1984. Light scattering by leaf layers with application to canopy reflectance modeling: the SAIL model. Remote Sens. Environ. 16 (2), 125–141.
Verhoeven, A.S., Adams III, W.W., Demmig-Adams, B., Croce, R., Bassi, R., 1999. Xanthophyll cycle pigment localization and dynamics during exposure to low temperatures and light stress in Vinca major. Plant Physiol. 120 (3), 727–738.
Vilfan, N., Van der Tol, C., Muller, O., Rascher, U., Verhoef, W., 2016. Fluspect-B: a model for leaf fluorescence, reflectance and transmittance spectra. Remote Sens. Environ. 186, 596–615.
Vilfan, N., Van der Tol, C., Yang, P., Wyber, R., Malenovský, Z., Robinson, S.A., Verhoef, W., 2018. Extending Fluspect to simulate xanthophyll driven leaf reflectance dynamics. Remote Sens. Environ. 211, 345–356.
Walker, A.P., Beckerman, A.P., Gu, L., Kattge, J., Cernusak, L.A., Domingues, T.F., Woodward, F.I., 2014. The relationship of leaf photosynthetic traits–Vcmax and Jmax–to leaf nitrogen, leaf phosphorus, and specific leaf area: a meta-analysis and modeling study. Ecol. Evol. 4 (16), 3218–3235.
Wang, Z., Skidmore, A.K., Darvishzadeh, R., Wang, T., 2018. Mapping forest canopy nitrogen content by inversion of coupled leaf-canopy radiative transfer models from airborne hyperspectral imagery. Agric. For. Meteorol. 253, 247–260.
Wang, Y., Suarez, L., Qian, X., Poblete, T., Gonzalez-Dugo, V., Ryu, D., Zarco-Tejada, P., 2021. Assessing the contribution of airborne-retrieved chlorophyll fluorescence for nitrogen assessment in almond orchards. In: Paper Presented at the 2021 IEEE International Geoscience and Remote Sensing Symposium. IGARSS.
Williams, C.K., Rasmussen, C.E., 1996. Gaussian Processes for Regression.
Williams, C.K., Rasmussen, C.E., 2006. Gaussian Processes for Machine Learning, Vol. 2. MIT press, Cambridge, MA.
Wood, C., Reeves, D., Duffield, R., Edmisten, K., 1992. Field chlorophyll measurements for evaluation of corn nitrogen status. J. Plant Nutr. 15 (4), 487–500.
Worton, B.J., 1989. Kernel methods for estimating the utilization distribution in home-range studies. Ecology 70 (1), 164–168.
Wu, C., Niu, Z., Tang, Q., Huang, W., 2008. Estimating chlorophyll content from hyperspectral vegetation indices: modeling and validation. Agric. For. Meteorol. 148 (8–9), 1230–1241.
Xiong, D., Chen, J., Yu, T., Gao, W., Ling, X., Li, Y., Huang, J., 2015. SPAD-based leaf nitrogen estimation is impacted by environmental factors and crop leaf characteristics. Sci. Rep. 5 (1), 1–12.
Yoder, B.J., Pettigrew-Crosby, R.E., 1995. Predicting nitrogen and chlorophyll content and concentrations from reflectance spectra (400–2500 nm) at leaf and canopy scales. Remote Sens. Environ. 53 (3), 199–211.
Zarco-Tejada, P.J., González-Dugo, V., Berni, J.A., 2012. Fluorescence, temperature and narrow-band indices acquired from a UAV platform for water stress detection using a micro-hyperspectral imager and a thermal camera. Remote Sens. Environ. 117, 322–337.
Zarco-Tejada, P.J., Morales, A., Testi, L., Villalobos, F.J., 2013. Spatio-temporal patterns of chlorophyll fluorescence and physiological and structural indices acquired from hyperspectral imagery as compared with carbon fluxes measured with eddy covariance. Remote Sens. Environ. 133, 102–115.
Zarco-Tejada, P.J., González-Dugo, M., Fereres, E., 2016. Seasonal stability of chlorophyll fluorescence quantified from airborne hyperspectral imagery as an indicator of net photosynthesis in the context of precision agriculture. Remote Sens. Environ. 179, 89–103.

Zarco-Tejada, P.J., Camino, C., Beck, P., Calderon, R., Hornero, A., Hernández-Clemente, R., Morelli, M., 2018. Previsual symptoms of Xylella fastidiosa infection revealed in spectral plant-trait alterations. Nat. Plants 4 (7), 432–439.
Zarco-Tejada, P.J., Poblete, T., Camino, C., Gonzalez-Dugo, V., Calderon, R., Hornero, A., Landa, B., 2021. Divergent abiotic spectral pathways unravel pathogen stress signals across species. Nat. Commun. 12 (1), 1–11.
Zebarth, B., Drury, C., Tremblay, N., Cambouris, A., 2009. Opportunities for improved fertilizer nitrogen management in production of arable crops in eastern Canada: a review. Can. J. Soil Sci. 89 (2), 113–132.